Development 140, 301-312 (2013) doi:10.1242/dev.084608

Developmentally coordinated extrinsic signals drive human pluripotent stem cell differentiation toward authentic DARPP-32$^+$ medium-sized spiny neurons

Alessia Delli Carri[1,*], Marco Onorati[1,*], Mariah J. Lelos[2], Valentina Castiglioni[1], Andrea Faedo[1], Ramesh Menon[3], Stefano Camnasio[1], Romina Vuono[4], Paolo Spaiardi[5], Francesca Talpo[5], Mauro Toselli[5], Gianvito Martino[3], Roger A. Barker[4], Stephen B. Dunnett[2], Gerardo Biella[5] and Elena Cattaneo[1,‡]

SUMMARY

Medium-sized spiny neurons (MSNs) are the only neostriatum projection neurons, and their degeneration underlies some of the clinical features of Huntington's disease. Using knowledge of human developmental biology and exposure to key neurodevelopmental molecules, human pluripotent stem (hPS) cells were induced to differentiate into MSNs. In a feeder-free adherent culture, ventral telencephalic specification is induced by BMP/TGFβ inhibition and subsequent SHH/DKK1 treatment. The emerging FOXG1$^+$/GSX2$^+$ telencephalic progenitors are then terminally differentiated, resulting in the systematic line-independent generation of FOXP1$^+$/FOXP2$^+$/CTIP2$^+$/calbindin$^+$/DARPP-32$^+$ MSNs. Similar to mature MSNs, these neurons carry dopamine and A2a receptors, elicit a typical firing pattern and show inhibitory postsynaptic currents, as well as dopamine neuromodulation and synaptic integration ability *in vivo*. When transplanted into the striatum of quinolinic acid-lesioned rats, hPS-derived neurons survive and differentiate into DARPP-32$^+$ neurons, leading to a restoration of apomorphine-induced rotation behavior. In summary, hPS cells can be efficiently driven to acquire a functional striatal fate using an ontogeny-recapitulating stepwise method that represents a platform for *in vitro* human developmental neurobiology studies and drug screening approaches.

KEY WORDS: DARPP-32 (PPP1R1B), Huntington's disease, Medium spiny neurons, Directed differentiation, Human embryonic stem cells, Striatal neuronal differentiation

INTRODUCTION

Early during central nervous system (CNS) development, morphologically distinct structures appear along the neuraxis. They constitute the prospective encephalic vesicles, the most anterior of which will give rise to the telencephalon. Coordinated patterning signals specify the dorsal telencephalon (pallium), which will give rise to multiple cortical structures, and the ventral telencephalon (subpallium), which is committed to forming the three ganglionic eminences, the septum, and the most ventral telencephalic stalk areas (Campbell, 2003; Schuurmans and Guillemot, 2002). The lateral and medial ganglionic eminences (LGE and MGE, respectively) give rise to different structures, the LGE being the source of the major neuronal populations of the striatum (Deacon et al., 1994; Olsson et al., 1995), which is composed mostly of medium-sized spiny neurons (MSNs) (Smith et al., 1998). MSNs are one of the first cells to undergo neurodegeneration in Huntington's disease (HD), an untreatable, dominantly inherited neurological disorder (Zuccato et al., 2010).

Human pluripotent stem (hPS) cells [both embryonic stem (ES) and induced pluripotent stem (iPS) cells] have emerged as a powerful tool for developmental biology studies, genetic and chemical screens and in regenerative medicine for neurological diseases, as they can generate a variety of neuronal subtypes (Gaspard and Vanderhaeghen, 2010).

Neural induction is the first step during neural development. This can be mimicked *in vitro* through embryoid body (EB) or stromal feeder co-culture (Liu and Zhang, 2011) and, more recently, by dual-SMAD signaling inhibition (Chambers et al., 2009). This latter strategy promotes rapid, massive and synchronous neural conversion of hPS cells in feeder-free and monolayer conditions. However, aspects of the specific striatal fate have thus far only been achieved in hES cells subjected to the undefined stromal co-culture method (Aubry et al., 2008) or in complex culture systems involving EB formation, giving rise to transplantable LGE-like progenitors of unverified definitive striatal character (Ma et al., 2012). In fact, none of these methods has documented the emergence of MSN progenitors from hPS cells that exhibit the correct combinatorial code of transcription factors and that lead to neuronal progeny exhibiting the neurochemical and electrophysiological characteristics expected of authentic human MSNs.

In this study, we developed an ontogeny-recapitulating protocol for the directed differentiation of hPS cells toward the striatal fate. We show that a dual-SMAD inhibition step drives neural induction and acquisition of a FOXG1$^+$/OTX2$^+$ identity. Sonic hedgehog (SHH) is relevant for the induction of ventral telencephalic fate (Lupo et al., 2006). We show that combinatorial SHH/WNT pathway modulation orchestrates the ventral telencephalic specification of hPS cells, committing FOXG1$^+$/OTX2$^+$ neural progenitors to 78% GABAergic cells among the MAP2ab$^+$ neuronal population, with a large proportion of CTIP2$^+$/calbindin$^+$ neurons. A definitive 20% of neurons are DARPP-32$^+$ MSNs, co-

[1]Center for Stem Cell Research, Università degli Studi di Milano, 20133 Milan, Italy. [2]School of Bioscience, Cardiff University, Cardiff CF10 3AX, UK. [3]Institute of Experimental Neurology (INSpe), Division of Neuroscience, San Raffaele Scientific Institute, Via Olgettina 58, 20132 Milan, Italy. [4]Brain Repair Centre, Department of Clinical Neuroscience, University of Cambridge, Cambridge CB2 0PY, UK. [5]Department of Biology and Biotechnology, University of Pavia, 27100 Pavia, Italy.

*These authors contributed equally to this work
‡Author for correspondence (elena.cattaneo@unimi.it)

Accepted 23 October 2012

expressing CTIP2 and carrying dopamine D2 and A2a receptors. Upon depolarization, these neurons elicit trains of action potentials and show consistent dopamine-dependent neuromodulation and synaptic integration *in vivo*. Moreover, we provide evidence for the survival and differentiation of the striatal precursors when grafted into a quinolinic acid-lesioned rat model of HD with correction of motor deficits.

MATERIALS AND METHODS

Cell culture and neuronal differentiation

hES (H9 and HS401) and hiPS [DF3F; see Camnasio et al. (Camnasio et al., 2012) and named WT-iPS 3F-1] cell lines were cultured as described (Camnasio et al., 2012). For neuronal induction, cells were plated as described (Chambers et al., 2009) at a density of 0.7×10^5 cells/cm^2 on Matrigel (Becton Dickinson)-coated dishes in mouse embryonic fibroblast (MEF)-conditioned hES cell medium supplemented with 10 ng/ml FGF2 and 10 μM Y-27632 (Sigma). Cell cultures were expanded for 3 days until confluent. The starting differentiation medium included KnockOut serum replacement medium (Invitrogen) supplemented with 5 μM dorsomorphin (Sigma) or 500 ng/ml noggin (R&D Systems) and 10 μM SB431542 (Tocris), which was used until day 12. Every 2 days, the medium was replaced with new medium containing an increasing proportion of N2 medium (25%, 50%, 75%). Starting on day 5, 200 ng/ml SHHC-25II (R&D Systems) and 100 ng/ml DKK1 (Peprotech) were added to the culture and maintained for 3 weeks. At day 15, the entire cell population was detached and replated on poly-lysine/laminin-coated dishes (Sigma-Aldrich). The cells were maintained in terminal differentiation medium, which comprised N2 medium supplemented with B27 and 30 ng/ml BDNF (Peprotech).

RNA isolation

Total RNA was prepared with Trizol (Invitrogen); human fetal brain RNA (Clontech) and human fetal striatum were used as positive controls. The RNA was treated with DNase I and purified using the RNeasy Kit (Qiagen). Then, 1 μg of total RNA was reverse-transcribed using SuperScript III reverse transcriptase and random primers according to the manufacturer's instructions (Invitrogen).

RT-PCR and RT-qPCR analysis

PCR was performed in a total volume of 25 μl containing 25 ng cDNA and using Taq polymerase (Invitrogen) according to the manufacturer's instructions. RT-PCR was performed in 30-35 cycles as described (Camnasio et al., 2012). Quantitative RT-PCR (RT-qPCR) was performed in triplicate and on two independent reverse transcriptase reactions for the genes analyzed using the CFX96 Real-Time System (Bio-Rad). All reactions were performed in 20 μl containing 50 ng cDNA and using iQ SYBR Green Supermix (Bio-Rad) as described (Marullo et al., 2010). Expressed Alu repeats (EARs) were used as reference for normalization (Marullo et al., 2010). Primers are described in supplementary material Table S1.

Microarray analysis

Total RNA was extracted from hES cell-derived samples at days 0, 15 and 45 of the protocol or from human LGE (hLGE) at different developmental ages (6 weeks, 6 weeks + 5 days, 7 weeks + 1 day) using the RNeasy Kit; 500 ng of total RNA from each sample was used for cRNA preparation using the Illumina TotalPrep RNA Amplification Kit (Ambion); 750 ng of labeled cRNAs were hybridized on Illumina HumanHT-12 v4 arrays (Illumina). The raw data were background subtracted and cubic spline normalized using Illumina GenomeStudio GX software. Detected probes were filtered with the detection criteria of $P<0.05$ in at least 25% of the samples. Differential gene expression analysis (day 0 versus day 15 or day 45) was performed using the linear model fit algorithm and empirical Bayes moderated test (Smyth, 2004) available in the R-Bioconductor platform. Multiple testing correction was conducted using the Benjamini-Hochberg method. The differentially expressed genes (DEGs) passed the $P<0.05$ and fold change of ≥1.7 thresholds.

The hierarchical cluster analysis was performed using Pearson's correlation (average linkage) implemented in the MeV package (Saeed et al., 2006). A subset of day-15 DEGs (subcluster) with a dissimilar trend in day-45 samples (and vice versa) was initially observed in the hierarchical cluster analysis. Further selection of subclusters was based on the comparison of expression levels relative to day 0. The gene ontology (GO) biological process enrichment analysis was performed using the GeneCodis tool (Nogales-Cadenas et al., 2009) with $P<0.05$ (hypergeometric test, corrected by the Benjamini-Hochberg method) and a minimum of three genes per GO term. Pathway enrichment analysis was performed using Ingenuity Pathway Analysis software (Ingenuity Systems) with a threshold of $P<0.05$ (Fisher's exact test, corrected by the Benjamini-Hochberg method). For the *in vitro* versus hLGE cluster analysis, the hLGE samples did not contribute to the average expression value for each DEG, but were challenged with the expression levels observed in the *in vitro* samples. The gene expression data are available at ArrayExpress with accession number E-MTAB-1080.

Immunodetection

Cells were fixed in 4% formaldehyde (FA), permeabilized with 0.5% Triton X-100 and blocked with 5% fetal bovine serum (FBS). Primary antibodies were incubated overnight at 4°C. Appropriate Alexa 488-, 568- or 647-conjugated secondary antibodies (Molecular Probes) were diluted 1:500 and mixed with Hoechst 33258 (5 μg/ml; Molecular Probes) to counterstain the nuclei. Images were acquired with a Leica DMI6000B microscope and analyzed with LAS-AF software, and then processed using Adobe Photoshop. Confocal images were acquired with a Zeiss LSM 510 microscope equipped with AIM4.2 software. For immunohistochemistry, brain tissue was sectioned to 40 μm and incubated as free-floating sections. Biotinylated secondary antibodies were used followed by visualization via DAB chromogen (Sigma-Aldrich). Antibodies are described in supplementary material Table S2.

Flow cytometry

Detached cells were fixed in 0.1% FA, permeabilized for 15 minutes in a 0.2% Tween 20 solution, resuspended in 50% FBS, and a solution containing primary antibodies added. For PAX6 staining, cells were fixed in cold 0.1% FA for 10 minutes at 4°C, permeabilized for 30 minutes with 90% methanol at 4°C and incubated overnight at 4°C. After washing, appropriate Alexa 488- and 647-conjugated secondary antibodies were used (1:1000). Primary isotypic antibodies were used as a control. Analysis was carried out using FACSCanto II and FACSDiva v6.1.3 software (BD Biosciences). For each analysis, 10,000 cells were analyzed. Antibodies are described in supplementary material Table S2.

Tissue collection

The human fetal tissues were from patients requesting termination of pregnancy. All procedures were approved by the Institutional Review Board (Comitato Etico) of the University of Milan and University of Cambridge, following full ethical review and approval in the UK in accordance with the Polkinghorne Report and Department of Health guidelines. Developmental stages of human fetuses were identified according to The Carnegie Institution for Science in Washington, DC, USA. The tissues were cut into 30 μm cryosections for immunostaining.

Electrophysiology

All recordings were performed using the whole-cell patch-clamp technique in voltage- and current-clamp configurations. The extracellular solution used to derive voltage signals and total ionic currents from neurons in culture is solution 1, whereas patch pipettes were filled with solution 2 (supplementary material Table S3). Cells were visualized using an inverted microscope (Nikon TE 200) and the signals were recorded as described previously (Onorati et al., 2011). Ligand-gated currents, elicited by the local application of GABA (20 μM), and GABAergic spontaneous postsynaptic currents (sPSCs) were derived as described (Mauri et al., 2012). To study dopaminergic modulation of GABA-elicited currents, 100 μM dopamine was co-applied with GABA. We also tested the effect of a selective D2 agonist (quinpirole, 5 μM) on membrane potential.

Recordings were performed in slices after transplantation. *In utero* transplantation was performed unilaterally in E16.5 rat fetuses with

100,000 GFP^+ day-45 differentiated striatal precursors. Animals (P15-27) were anesthetized with isofluorane and decapitated. The whole brain was quickly removed and submerged in ice-cold carboxygenated solution 4 (supplementary material Table S3). Then, 300 μm coronal slices were prepared using a vibratome and transferred to an incubation chamber filled with carboxygenated aCSF solution 5 (supplementary material Table S3). During recordings, neurons were visualized using an upright microscope (Nikon Eclipse 600N) equipped with an epifluorescence device and connected to a near-infra red CCD camera. Membrane potential, total ionic current and PSCs were recorded using extracellular solution 5 and the pipettes were filled with solution 2. Recordings were made with a MultiClamp 700B amplifier and digitized with a Digidata 1322 computer (Molecular Devices). Data were acquired using Clampex 9.2 (Axon Instruments), sampled at 20 kHz and filtered at 10 kHz. Biocytin (Sigma-Aldrich) was intracellularly injected through the pipette during recordings. Solutions 1-5 are described in supplementary material Table S3.

Transplantation

Animal experiments were conducted under protocols approved by the Caltech Institutional Animal Care and Use Committee. Cell suspensions were transplanted into nine female Lister hooded rats. Rats received unilateral quinolinic acid lesions to the right hemisphere at the following coordinates (AP, anteroposterior; ML, mediolateral; DV, dorsoventral): (1) AP +0.4, ML –3.4, DV –4.5/–3.5; and (2) AP +1.4, ML –2.8, DV –4.5/–3.5. Eight days post-lesion, a daily regimen of cyclosporin A immunosuppression was initiated (1 mg/kg by intraperitoneal injection). The following day, 500,000 day-38 differentiated cells were injected (2 μl by volume) bilaterally into the lesion and intact hemispheres at the following coordinates: AP +0.9, ML +3.1/–3.1, DV –4.5/–3.5. At 3, 6 and 9 weeks post-transplant, rats were perfused transcardially under euthal anesthesia. After exsanguinations with phosphate-buffered saline, tissue was fixed with 1.5% FA and stored in 1.5% FA for an additional 24 hours before transfer to 25% reagent-grade sucrose solution in distilled H_2O.

Apomorphine-induced rotations

At 3 weeks post-lesion and prior to perfusion, rats were injected subcutaneously with 1 mg/kg apomorphine (dissolved in 0.9% saline; Sigma). They were placed in automated rotometer bowls, based on the design of Ungerstedt and Arbuthnott (Ungerstedt and Arbuthnott, 1970; Torres et al., 2008) and movements were recorded for 60 minutes. The data are reported as net contralateral scores (contralateral minus ipsilateral counts) over each test session.

RESULTS

hPS cells acquire a ventral telencephalic fate when exposed to extrinsic developmental signals

Positional information is a general feature that organizes cellular identities on the basis of their anatomic location in multicellular organisms. Combinatorial codes of transcription factors are expressed over time in each progenitor domain, thus specifying distinct CNS compartments.

Using knowledge of human developmental biology, we followed the temporal expression pattern of relevant developmental markers during hPS cell differentiation *in vitro*. We showed that the 11-week-old developing human telencephalon expresses the forebrain/midbrain marker OTX2 (Fig. 1A) (Nat and Dechant, 2011), as well as the telencephalic marker FOXG1 (Manuel et al., 2010) (Fig. 1B). In the subpallium, the ventricular and subventricular zones (VZ and SVZ, respectively) of the LGE already express the key regional marker GSX2 (Fig. 1C), identifying early striatal progenitors that will give rise to MSNs (Nat and Dechant, 2011) (Fig. 1D,E).

In the present study we sought to design a monolayer, feeder-free, stepwise protocol that allows hPS cells to progress through $OTX2^+/FOXG1^+/GSX2^+$ stages, ultimately leading to the striatal fate (Fig. 1F). The protocol comprises three phases: neural induction, regionalization, and terminal differentiation. These phases mimic the normal neurodevelopment of the ventral telencephalon (Fig. 1F).

For neural induction, we exposed hPS cells to the synergistic dual inhibition of SMAD signaling by noggin (N) and SB431542 (SB), as described (Chambers et al., 2009). We used dorsomorphin (D), an inhibitor of BMP, which has also been shown to induce rapid and highly efficient neural conversion (Zhou et al., 2010), interchangeably in combination with SB (N+SB or D+SB) and observed a comparable neural conversion efficiency (supplementary material Fig. S1A-C), as was also the case with the noggin analog LDN-193189 (supplementary material Fig. S1D).

Neuroepithelial cells progress toward telencephalic identity through stages of rostrocaudal (RC) and dorsoventral (DV) patterning. Commitment to the ventral telencephalic fate is regulated by the temporal coordination of ventralizing morphogens such as SHH (Ericson et al., 1995; Kohtz et al., 1998). Furthermore, hES cell-derived telencephalic progenitors can also be efficiently patterned toward the ventral fate through simultaneous modulation of the WNT pathway by dickkopf 1 (DKK1) (Li et al., 2009).

Neural induction of hPS cells was achieved by exposure to D+SB for 12 days and demonstrated by the formation of neural rosettes (Zhang et al., 2001) at day 15 (Fig. 1H). Beginning at day 5, regional patterning was achieved with a coordinated regimen that employed DKK1 and a modified version of SHH (SHH C-25II). This regimen was applied for the following 3 weeks and then the cells were terminally differentiated for up to 80 days, giving rise to an elaborate network of fibers (Fig. 1I,J). We demonstrated that this morphogen exposure was able to significantly induce a ventral telencephalic fate. We adopted the ratio of *EMX2* (a dorsal pallial marker) to *NKX2-1* (an MGE marker) expression as an index of DV identity. In the presence of morphogens (+F) the DV index was shifted toward a ventral fate, in comparison to the absence of morphogen (–F) (Fig. 1K).

To monitor neural conversion and patterning, we first analyzed the expression profile of a set of diagnostic neuroectodermal and regional markers by RT-PCR (supplementary material Fig. S1E). The early neuroectodermal genes *PAX6* and *SOX1* (Zhang et al., 2010) and the rosette markers *DACH1*, *LIX1*, *LMO3* and *MSX1* (Elkabetz et al., 2008; Koch et al., 2009) were expressed from day 5. The analysis of a panel of RC and DV markers showed that the rostral markers *OTX1*, *OTX2* and *SIX3* (Appolloni et al., 2008; Nat and Dechant, 2011) and the ventral telencephalic genes *DLX5*, *DLX6* and *ASCL1* (Nat and Dechant, 2011) were correctly expressed and, after day 5, the expression of the caudal marker *GBX2* decreased (supplementary material Fig. S1E). Altogether, this expression profile suggests that neural progenitors were entering a ventral telencephalic regional specification program consistent with *in vivo* events. This was confirmed through immunofluorescence analysis. OCT4 (POU5F1 – Human Gene Nomenclature Committee) was lost starting from day 5 (Fig. 1L′), whereas cells continued to express the neuroectodermal marker OTX2 (Fig. 1L-L″), PAX6 and nestin at high levels (Fig. 1M-M″). In agreement with previous studies (Li et al., 2009; Zhang et al., 2010), we observed SOX1 protein expression at day 15, following PAX6 (Fig. 1N″). The broadly telencephalic identity of these cells was confirmed by the expression of FOXG1 (58% of cells), and ventral specification was confirmed by GSX2 immunopositivity (67% of cells) (Fig. 1O,P).

Flow cytometric analysis confirmed the pluripotent-to-neuropotent transition by showing an 88% increase in neuroectodermal $OTX2^+/OCT4^-$ cells and PAX6 expression in 64% of cells at day 15 (Fig. 1Q).

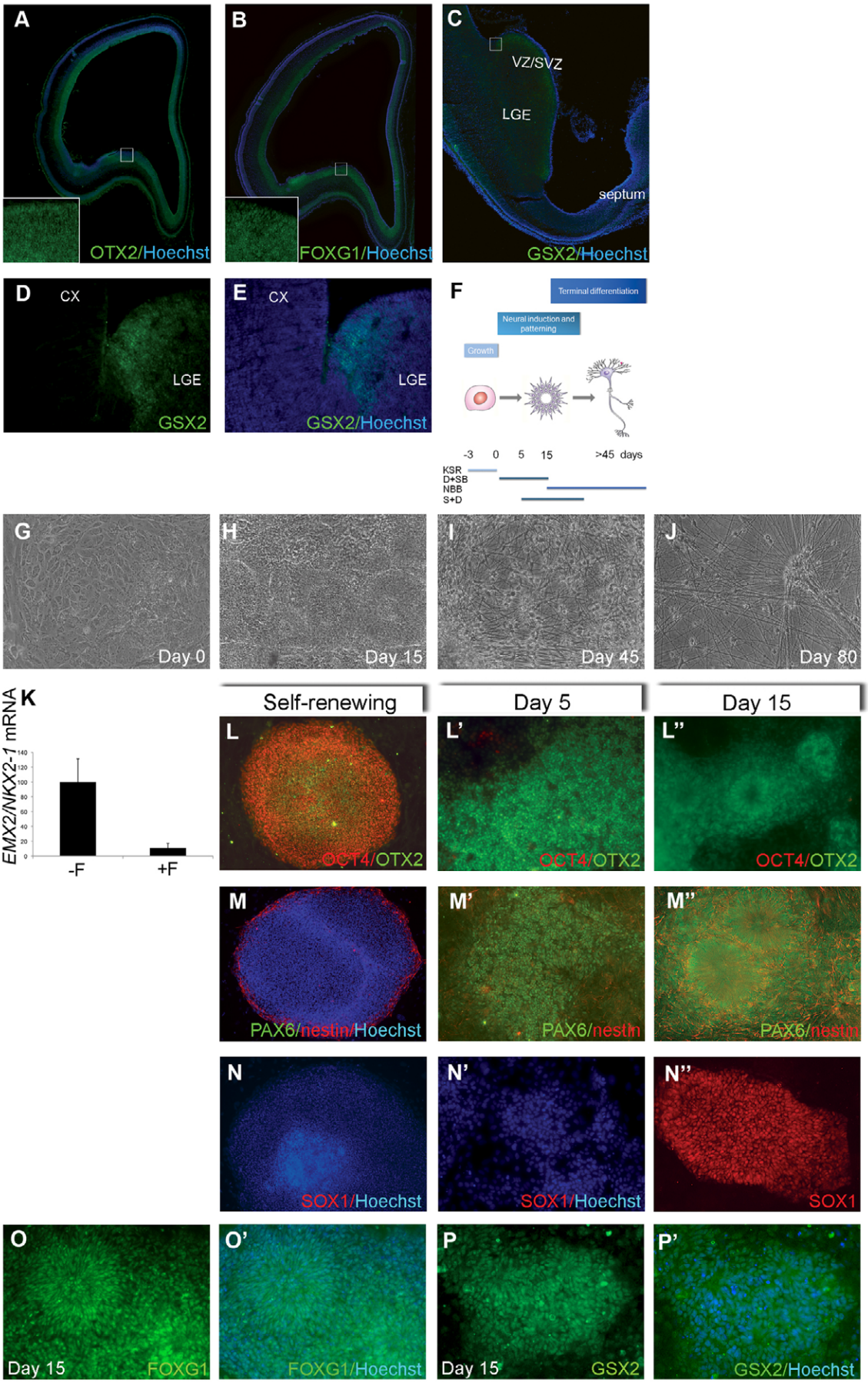
A
OTX2/Hoechst
B
FOXG1/Hoechst
C
VZ/SVZ
LGE
septum
GSX2/Hoechst
D
CX
LGE
GSX2
E
CX
LGE
GSX2/Hoechst
F
Terminal differentiation
Neural induction and patterning
Growth
-3 0 5 15 >45 days
KSR
D+SB
NBB
S+D
G
Day 0
H
Day 15
I
Day 45
J
Day 80
K
EMX2/NKX2-1 mRNA
-F
+F
Self-renewing
Day 5
Day 15
L
OCT4/OTX2
L'
OCT4/OTX2
L''
OCT4/OTX2
M
PAX6/nestin/Hoechst
M'
PAX6/nestin
M''
PAX6/nestin
N
SOX1/Hoechst
N'
SOX1/Hoechst
N''
SOX1
O
Day 15
FOXG1
O'
FOXG1/Hoechst
P
Day 15
GSX2
P'
GSX2/Hoechst

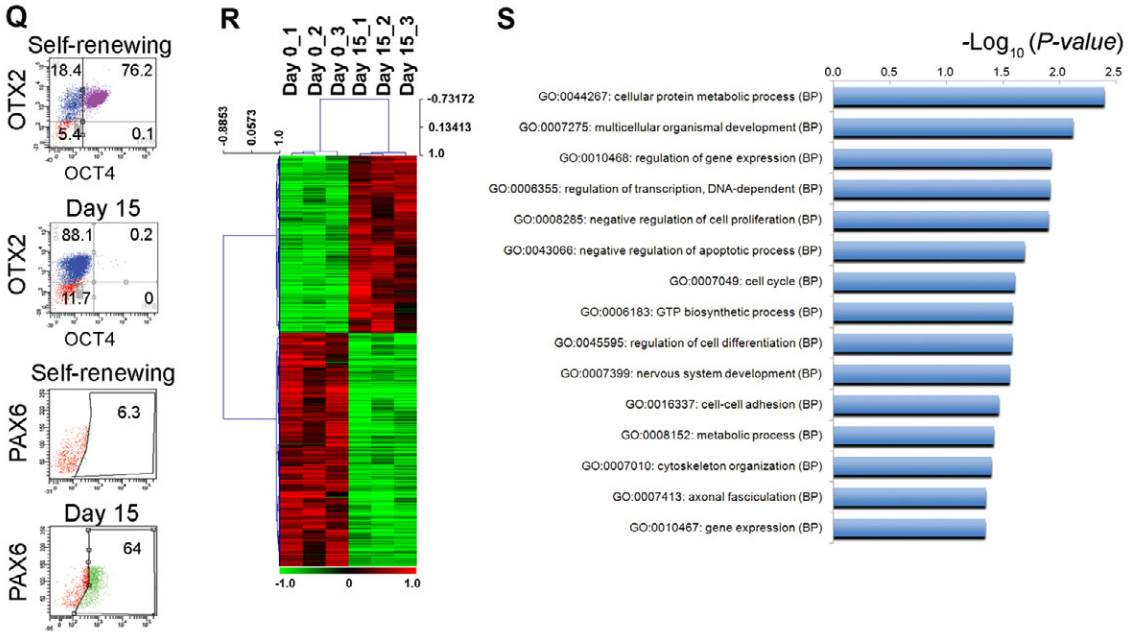

Fig. 1. Neural conversion of hES cells to ventral telencephalic progenitors. (**A-C**) Immunocytochemistry on coronal sections of 11-week-old human fetal telencephalon. OTX2 (A) and FOXG1 (B) show broad expression in the telencephalic vesicle. The boxed regions are shown at higher magnification in the insets, which illustrate OTX2 and FOXG1 expression in the germinal zones. (C) GSX2 is specifically expressed in the LGE. (**D**,**E**) Higher magnification of the boxed region in C. (**F**) The differentiation protocol. D+SB, dorsomorphin and SB431542; KSR, KnockOut serum replacement medium; NBB, N2 B27 BDNF medium; S+D, SHH and DKK1. (**G-J**) Stages of the differentiation. (**K**) Dorsoventral identity acquisition during the neural induction phase is shown by the *EMX2*/*NKX2-1* ratio at day 15 in the presence of morphogens SHH and DKK1 (+F) versus no morphogens (–F). Mean ± s.d. of three experiments. Data are expressed as a percentage of –F. (**L-N″**) Immunofluorescent staining during neural induction for OCT4/OTX2 (L-L″), PAX6/nestin (M-M″) and SOX1 (N-N″). (**O**,**O′**) Immunodetection at day 15 of FOXG1; 58±7.5% of cells expressed FOXG1 (*n*=3292 cells, three experiments). (**P**,**P′**) Immunodetection at day 15 indicates that 63.7±8% of cells (*n*=3570 cells) are GSX2$^+$. (**Q**) Flow cytometry in self-renewal conditions versus day 15 for OCT4/OTX2 and PAX6. (**R**) Transcriptional signature discriminating day-15 versus day-0 samples (*n*=3 each). (**S**) Selection of enriched and neural-related GO classes obtained from gene enrichment analysis using GeneCodis. BP, biological process; CX, cortex; LGE, lateral ganglionic eminence; VZ/SVZ, ventricular/subventricular zones. Original magnifications: 5× in A-C; 10× in G-J; 20× in A,B insets, D,E,L-P′. The experiments described were performed on the hES H9 cell line.

In parallel, an unsupervised systematic analysis was performed using genome-wide gene expression profiling. Hierarchical clustering of differentially expressed genes segregated day-15 neural progenitors and hES cells (Fig. 1R; supplementary material Table S4). Gene enrichment analysis revealed gene ontology (GO) classes related to nervous system development and cytoskeleton/axonal organization (Fig. 1S). Ingenuity pathway analysis identified pluripotency downregulation at day 15 and subsequent time points (supplementary material Fig. S2A). Subclustering analysis identified candidate stage-specific striatal enriched transcripts (supplementary material Fig. S2B and Table S4), including *LIX1*, *ZNF503* (*NOLZ1*) and *CXCR7*, which were validated using the Allen Brain Atlas human gene expression database (supplementary material Fig. S2C).

Next, we determined whether the protocol that we had developed could be reliably applied to different hPS cell lines. We cross-compared H9 and HS401 hES cell lines with DF3F hiPS cells. After 15 days, the HS401 hES cell line strongly expressed OTX2, PAX6, nestin, SOX1 and FOXG1 (supplementary material Fig. S3A-F). The DF3F hiPS cell line was exposed to the same protocol, leading to an analogous neural fate at day 15 (supplementary material Fig. S3G-M). Furthermore, we verified that D+SB treatment suppressed non-CNS fates (supplementary material Fig. S4A-F).

We conclude that the combined action of developmentally regulated neural inductive and patterning signals is able to push different lines of hPS cells toward neural progenitors that exhibit characteristics compatible with a ventral telencephalic identity.

Early differentiation of ventral telencephalic progenitors yields GABAergic neurons of MSN identity

Our *in vivo* human study showed that the transcription factors FOXP1 and FOXP2 are expressed in the LGE domain of the 11-week-old fetus, labeling striatal precursors and differentiated MSNs (Fig. 2A,B). CTIP2 (BCL11B) is uniquely expressed in the mouse striatum by MSNs, specifically labeling this neuronal population from early postmitotic stages (Arlotta et al., 2008). We show that at 11 weeks of human development, CTIP2 is expressed in the striatal anlage. Moreover, CTIP2$^+$ neurons in the caudate nucleus co-expressed the MSN-specific marker DARPP-32 (PPP1R1B – Human Gene Nomenclature Committee), which is present in 95% of MSNs and is not expressed by other cell types within the striatum (Ouimet et al., 1998; Ouimet et al., 1984) (Fig. 2C,D).

In vitro, at day 45 of neural differentiation, βIII-tubulin$^+$ neuronal cells (80% of cells) with branched MAP2ab$^+$ (ab refers to the two isoforms of the protein present in mature neurons) and TAU$^+$ (MAPT – Human Gene Nomenclature Committee) neurites started to form a neuronal network (Fig. 2E,F). The majority of these neurons exhibited a GABAergic phenotype, an expected result of ventral telencephalic specification that was confirmed by immunocytodetection of GAD65/67 (GAD2/1 – Human Gene

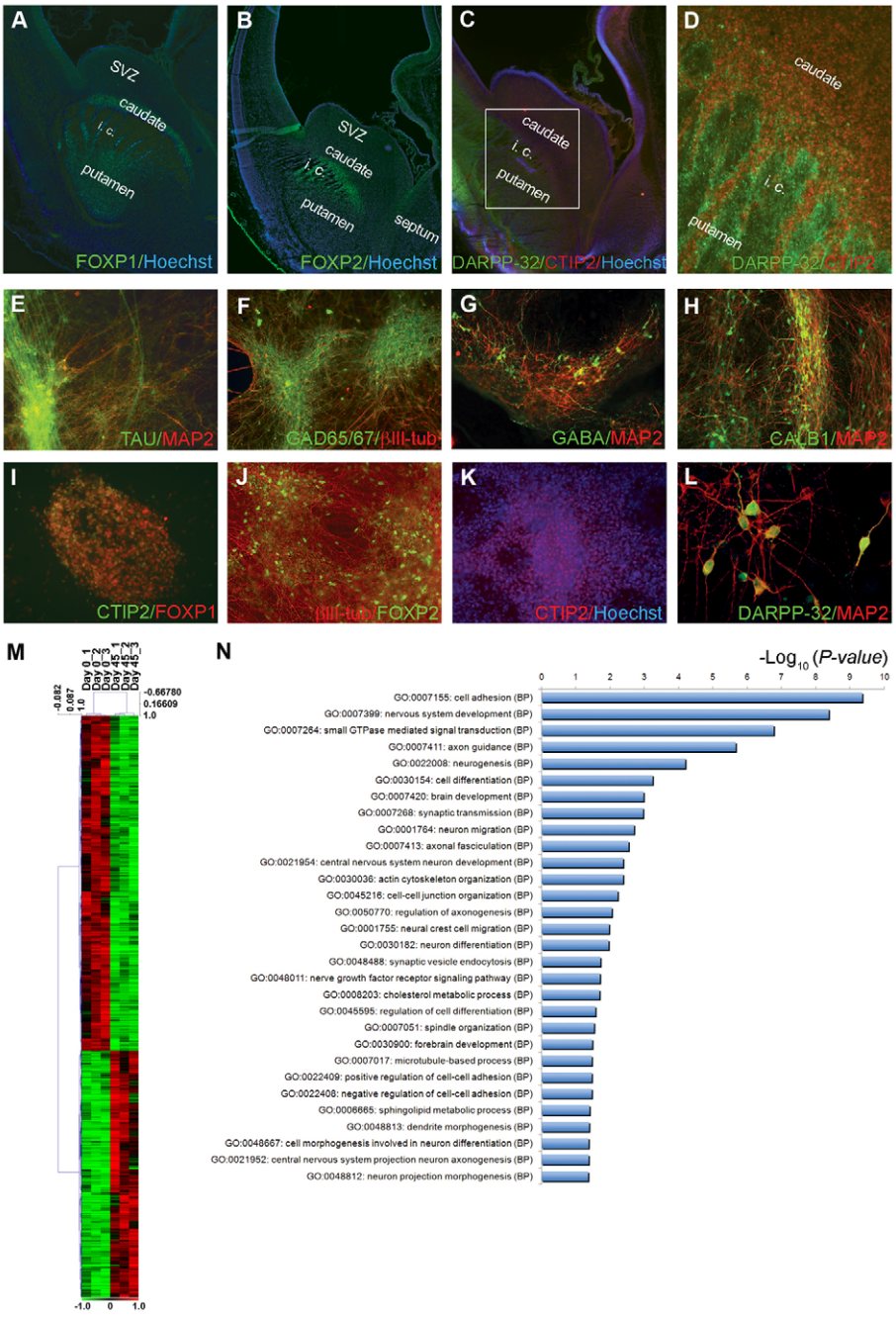

Fig. 2. The differentiation protocol induces GABAergic differentiation of MSNs after 45 days. (**A-D**) Coronal sections of 11-week-old human fetal telencephalon. Shown are FOXP1$^+$ (A) and FOXP2$^+$ (B) striatal precursors in the caudate nucleus and putamen. (C,D) Immunostaining for CTIP2 and DARPP-32. (D) Higher magnification of the boxed region in C. (**E**) Expression of the pan-neuronal markers MAP2ab and TAU at day 45. (**F-H**) Immunodetection of GAD65/67 and βIII-tubulin (F); MAP2ab$^+$ neurons express GABA (G) and calbindin (CALB1) (H) at day 45. (**I**,**J**) Double labeling of cells for FOXP1/CTIP2 and FOXP2/βIII-tubulin in differentiated striatal cells at day 45. (**K**) The early postmitotic striatal marker CTIP2 is expressed in neuronal cells at day 45. (**L**) Confocal image of MAP2ab$^+$ neurons expressing DARPP-32 at day 45. (**M**) Transcriptional signature differentiating day-45 versus day-0 samples (n=3 each). (**N**) Selection of mature neuronal function-related GO classes obtained from gene enrichment analysis using GeneCodis. i. c., internal capsule. Original magnifications: 5× in A-C; 20× in D-K; 40× in L. The experiments described were performed on the hES H9 cell line.

Nomenclature Committee), GABA and calbindin (CALB1) (Fig. 2F-H). At this stage, striatal precursors were positive for FOXP1, FOXP2 and CTIP2 (Fig. 2I-K), and differentiated DARPP-32$^+$ MSNs began to appear (Fig. 2L). No SOX1$^+$ early neural progenitors were detectable at this stage (data not shown).

Genome-wide transcriptome studies confirmed an overall neuronal fate switch in the transcriptional signature of day-45 differentiated cells (Fig. 2M). Gene enrichment analysis provided several neuronal-related GO classes, such as ‘synaptic transmission’ and ‘forebrain development’ (Fig. 2M,N). Subclustering analysis identified stage-specific enriched transcripts relevant to synaptic function, tight junctions and cell adhesion or striatal fate (supplementary material Fig. S5A,B), including *EBF1*, *ASCL1*, *GBX2* and *SOX5* (supplementary material Fig. S5C and Table S4).

To prove that the *in vitro* transcriptional changes corresponded to those occurring during human ventral forebrain development, we performed global gene expression profiling of three human fetal LGE samples (gestational ages between 6 and 7 weeks). In the unsupervised cluster analysis using the day-15 and day-45 signatures, the hLGE group was positioned as a sub-branch with the day-15 or day-45 group, which in both cases clearly separated from the day-0 group (supplementary material Fig. S6A,B).

Generated MSNs acquire complete antigenic and terminal maturation by day 80

We differentiated the cells until day 80 and analyzed the temporal gene expression profile for diagnostic transcription factors. After the early expression of *FOXG1*, postmitotic striatal precursors begin to express *ISL1*, which then disappears in mature MSNs but

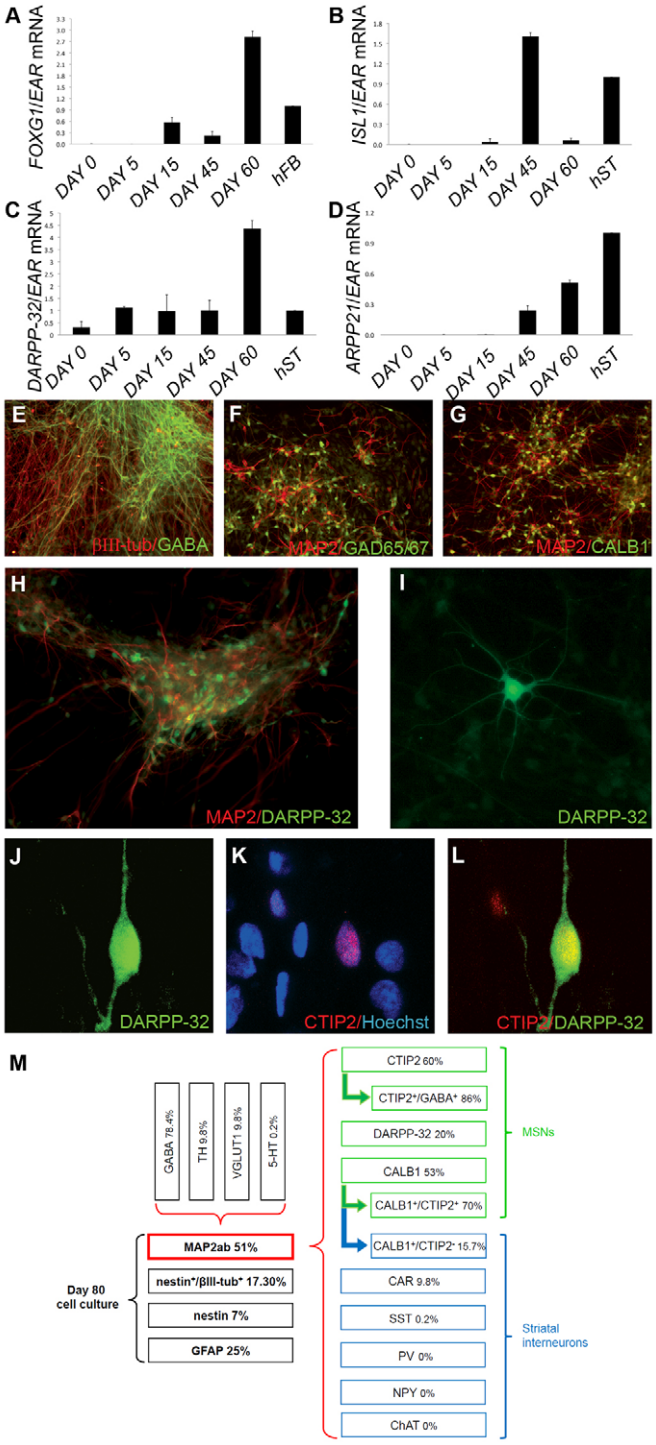

Fig. 3. Generation of differentiated MSNs after day 80. (**A-D**) RT-qPCR analysis for *FOXG1* (A), *ISL1* (B), *DARPP-32* (C) and *ARPP21* (D). Mean ± s.d. of three experiments. Data were normalized to expressed Alu repeat (*EAR*) mRNA. RNA from human fetal striatum (hST) or total fetal brain (hFB) was used as control. (**E-G**) Mature neurons exhibit a GABAergic identity. (**H**) DARPP-32$^+$ neurons form large fields. (**I**) High magnification showing typical DARPP-32$^+$ MSN morphology. (**J-L**) Confocal analysis confirming MSN identity by co-expression of CTIP2 and DARPP-32. (**M**) Description of the different neuronal populations. MAP2ab$^+$ 51±3%, *n*=1126 cells; GFAP$^+$ 25±0.03%, *n*=712; nestin$^+$/βIII-tubulin$^+$ 17.3±5.03%, *n*=208; nestin$^+$ 7±4.9%, *n*=220; GABA$^+$ 78.4±9.8%, *n*=1242; tyrosine hydroxylase (TH)$^+$ 9.8±0.98%, *n*=826; VGLUT1$^+$ 9.8±0.6%, *n*=1005; 5-hydroxytryptamine (5-HT)$^+$ 0.2±0.02%, *n*=775; CTIP2$^+$ 60.3±14.1%, *n*=320; CTIP2$^+$/GABA$^+$ 86±7.6%, *n*=320; CALB1$^+$ 53±5%, *n*=1020; CALB1$^+$/CTIP2$^+$ 70.6±19.5%, *n*=770; DARPP-32$^+$ 20±3.9%, *n*=987; CALB1$^+$/CTIP2$^-$ 29.4±19.5%, *n*=770; calretinin (CAR)$^+$ 9.8±3.9%, *n*=956; SST$^+$ 0.2±0.02%, *n*=810; PVALB$^+$ 0%, *n*=790; NPY$^+$ 0%, *n*=680; ChAT$^+$ 0%, *n*=540) (mean ± s.d.). Original magnifications: 20× in E-H; 40× in I-L. The experiments described were performed on the hES H9 cell line.

persists in cholinergic interneurons (Wang and Liu, 2001). RT-qPCR analysis confirmed *FOXG1* expression starting at day 15 and persisting during terminal differentiation, achieving strong expression at day 60 (Fig. 3A). *ISL1* reached peak expression at day 45 and decreased thereafter (Fig. 3B). Expression of the MSN markers *ARPP21* and *DARPP-32* (Girault et al., 1990) gradually increased starting from day 45 and persisted throughout the differentiation process (Fig. 3C,D). Collectively, these data confirm that *in vitro* cell transition toward a mature phenotype exhibited a temporal profile consistent with that of *in vivo* expression.

At the end of the differentiation period, we performed a general antigenic categorization of the cell types present in the culture. Fifty-one percent of cells were MAP2ab$^+$ neurons (Fig. 3F,M; supplementary material Fig. S7C). βIII-tubulin$^+$ neurons formed a complex neuronal layer, and 17% of total cells were double positive for nestin, suggesting a neuronal precursor identity (Fig. 3M; supplementary material Fig. S7A,C). Only 7% of the total cells were pure nestin$^+$ progenitors (Fig. 3M; supplementary material Fig. S7A,C). The protocol also allowed late astrogliogenesis, as GFAP$^+$ cells appeared only around day 80 (25% of cells) (Fig. 3M; supplementary material Fig. S7B,C). With respect to the MAP2ab$^+$ neurons, 78% were GABA$^+$, 60.3% CTIP2$^+$ (86% of which co-expressed GABA) and 53% CALB1$^+$ neurons. We found that 70.6% of the CALB1$^+$ neurons co-expressed CTIP2 (Fig. 3M; supplementary material Fig. S7D,E), thus confirming the general acquisition of an MSN fate. An estimated 20% of the neurons were immunopositive for DARPP-32 (Fig. 3H,M). MSN identity was also corroborated by confocal analysis for DARPP-32 and CTIP2 co-expression (Fig. 3J-L).

At the end of differentiation, HS401 hES cells also generated FOXP2$^+$ cells and DARPP-32$^+$ neurons with an efficiency comparable to that of the H9 hES cell line (supplementary material Fig. S8A-C,J). Similarly, hiPS cells differentiated promptly, giving rise to GABAergic neurons (supplementary material Fig. S8D-G,J) and DARPP-32$^+$/CTIP2$^+$ MSNs (supplementary material Fig. S8H-J). These data demonstrate that our protocol is applicable to multiple hES and iPS cell lines.

The striatal interneuronal populations, most of which are GABAergic with different histochemical phenotypes [positive for calretinin (CR; calbindin 2), parvalbumin (PVALB), somatostatin (SST) or neuropeptide Y (NPY)/nitric oxide synthase (NOS)], also arise from the ventral telencephalic eminences (Kreitzer, 2009), together with a small population of cholinergic interneurons. In our neuronal cultures, CALB1$^+$/CTIP2$^-$ cells account for 15.7% (Fig. 3M; supplementary material Fig. S7E), suggesting their striatal non-MSN identity. Approximately 9.8% of cells were CR$^+$ (Fig. 3M; supplementary material Fig. S7F). We found a few SST$^+$ interneurons (Fig. 3M; supplementary material Fig. S7G), but no NPY$^+$, PVALB$^+$ (Fig. 3M; supplementary material Fig. S7F,G) or choline O-acetyltransferase (ChAT)$^+$ interneurons (not shown).

Only a few non-striatal neuronal subtypes were present (Fig. 3M; supplementary material Fig. S7H,I). By contrast, the condition without morphogens (–F) generated almost exclusively VGLUT1$^+$ (SLC17A7 – Human Gene Nomenclature Committee) neurons and no DARPP-32$^+$ cells were found (supplementary material Fig. S9A,B).

Next, we examined whether the generated MSNs exhibit molecular and neurochemical characteristics similar to those of authentic endogenous MSNs. Based on their dopamine receptor expression, MSNs form the direct and indirect pathways of the basal ganglia circuits (Kreitzer, 2009). Using RT-qPCR, we observed that the dopamine receptor *DRD1* gene was highly expressed from day 45 (Fig. 4A). The presence of DRD2 was detected in βIII-tubulin$^+$ neurites (Fig. 4B) and, more specifically, in CTIP2$^+$ MSNs (Fig. 4C). We also detected expression of the A2a receptor (Fig. 4D). These data demonstrate that the *in vitro*-generated neurons acquire several of the molecular and neurochemical characteristics typical of authentic MSNs.

Development of sodium currents, firing of action potentials and functional GABA receptors in neuronal progeny

A distinctive feature of fully differentiated hES/iPS cell-derived neurons is their ability to fire action potentials. Subclustering analysis of gene expression data at day 45 revealed transcript enrichment in a number of voltage-gated ion channel subunits, such as voltage-gated Na$^+$ channel α- and β-subunits (supplementary material Fig. S5), suggesting that these cells might be able to elicit action potentials. Particularly interesting is the over 6-fold increase in the transcript that encodes Nav1.2 (SCN2A – Human Gene Nomenclature Committee), an α-subunit Na$^+$ channel subtype implicated in action potential initiation and conduction and in repetitive firing.

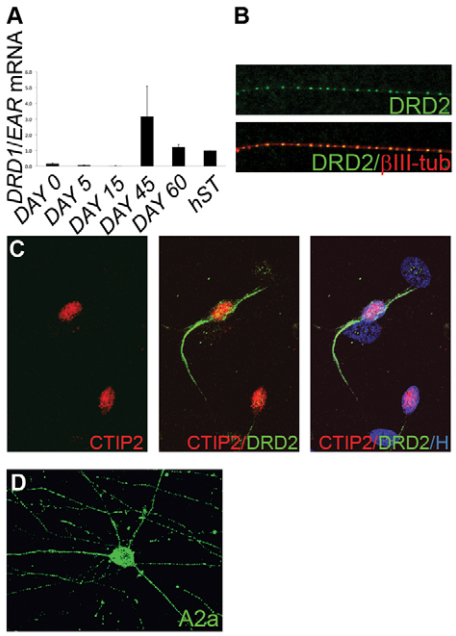

Fig. 4. Molecular and antigenic investigation of the differentiating striatal cultures. (**A**) RT-qPCR analysis of *DRD1*. Mean ± s.d. of three experiments. Data were normalized to *EAR* mRNA. hST, human fetal striatum RNA control. (**B**,**C**) Confocal analysis for DRD2 with βIII-tubulin (B) and CTIP2 (C) at day 80. H, Hoechst. (**D**) Confocal image of immunostaining for A2a receptor at day 80. Original magnifications: 40×. The experiments described were performed on the hES H9 cell line.

We evaluated the electrophysiological properties of hES cell-derived differentiated neurons through the whole-cell patch-clamp technique in both voltage- and current-clamp modes. We found that 13% of the recorded neurons did not show any regenerative event during stimulation with a suprathreshold rectangular depolarizing step of current, 30% elicited a single action potential and 57% showed repetitive firing (Fig. 5A, mean in 5D). In parallel, we found a correlation between the ability of these cells to elicit action potentials and the activation of sizeable voltage-gated fast Na$^+$ and delayed-rectifier K$^+$ currents [Fig. 5B, where a family of total inward and outward currents is presented, obtained from the same cell as shown in Fig. 5A then post-marked with biocytin and for DARPP-32 (Fig. 5C)]. Na$^+$ currents were elicited at test potentials ranging between –70 and +40 mV from a holding potential of –90 mV. In ~19% of the recorded cells, the amplitude of the Na$^+$ current was negligible, in 26% of cells current peak amplitude ranged between 0 and 400 pA, and in ~55% of cells it was greater than 400 pA (Fig. 5E). Cell capacitance (29.43±5.27 pF) and input resistance (944±125 MΩ) did not vary significantly among the three groups described above. Among the neurons able to sustain repetitive firing, 85% (11 out of 13) yielded a slow depolarization and a delay in generating the initial spike (Fig. 5F, inset), just as described for rat MSNs (Nisenbaum et al., 1996; Shen et al., 2004; Surmeier et al., 1989; Surmeier et al., 1991). This behavior suggests that, in those cells that show a delayed onset in generating the first spike, a fast inactivating K$^+$ current should also be elicited that has properties that resemble those of the I_A current involved in firing frequency regulation and first spike latency (Ericsson et al., 2011; Jiang and North, 1991), a hallmark of MSNs.

Next, we assessed whether ligand-gated channels expressed in these cells could be activated by application of inhibitory or excitatory neurotransmitters, as would occur in a functional synaptic network. After local GABA application, GABA-evoked currents were observed in 74% of recorded cells. Since RT-qPCR and immunofluorescence indicated the presence of dopaminergic receptors, we investigated a possible modulatory effect of dopamine on GABA-elicited currents. In three out of five cells, dopamine significantly, and partially reversibly, reduced the peak of the GABA-evoked current by 27±10% (Fig. 5G).

The general excitability of neurons in culture and the functionality of the synaptic network were investigated by analyzing the presence of spontaneous postsynaptic currents (sPSCs). Since the hES cell-derived differentiated neurons show a rather depolarized resting potential (mean –43±4.9 mV) and no spontaneous action potentials were recorded at resting, we expected to observe spontaneous GABAergic currents at a very low frequency, if at all. Indeed, very low frequency GABAergic sPSCs were observed in three hES cell-derived differentiated neurons (Fig. 5H), whereas glutamatergic sPSCs were not detected (Fig. 3M). The presence of mature synapses was also demonstrated by confocal immunodetection of synaptophysin (Fig. 5I).

hiPS cell-derived differentiated neurons were also analyzed (supplementary material Fig. S10A). We found that 55% generated currents greater than 400 pA (supplementary material Fig. S10G) and, during suprathreshold depolarization, 39% generated repetitive firing (supplementary material Fig. S10B,H). Application of the selective D2 agonist quinpirole induced hyperpolarization of the membrane potential in two out of four cells, which is consistent with a D2-mediated modulation of K$^+$ channels (Kuzhikandathil et al., 1998; Lavine et al., 2002; Beaulieu and Gainetdinov, 2011).

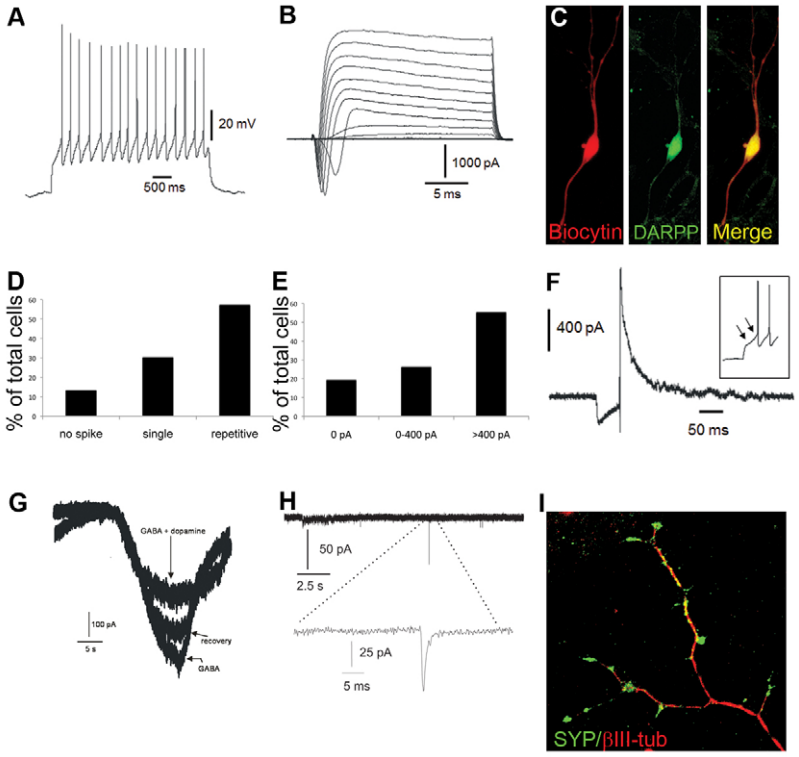

Fig. 5. Electrophysiological properties of differentiated neurons. (**A**) Sample trace of a repetitive firing in 87-day differentiated neurons when excited with a suprathreshold depolarizing step of current. (**B**) Family of total inward and outward currents. (**C**) Confocal image of a recorded biocytin$^+$/DARPP-32$^+$ cell. (**D**,**E**) The fraction of cells subdivided according to their firing properties (D) (no spike 13%, *n*=3 cells; single spike 30%, *n*=7; repetitive firing 57%, *n*=13) or amplitude of the Na^+ current peak (E) [0 pA 19%, *n*=11 cells; <400 pA (–218±25 pA) 26%, *n*=15; >400 pA (–1750±250 pA) 55%, *n*=32 (mean ± s.e.m.)]. (**F**) A proportion of the cells (23%, *n*=11 cells) showed a fast inactivating K^+ current with properties that resemble those of I_A. The onset delay in the generation of the first spike (inset, arrows) is a typical electrophysiological property of mature MSNs. (**G**) Local application of GABA at –80 mV elicits an inward current with a mean amplitude of 357±160 pA in 74% of recorded neurons. In a fraction of the responding cells, this amplitude was significantly (27±10%) reduced by co-application of dopamine. This effect was partially reversible. (**H**) GABAergic spontaneous postsynaptic currents (sPSCs) recorded in three cells (mean amplitude of 61±16 pA). (**I**) Confocal image of immunostaining for synaptophysin (SYP) and βIII-tubulin at day 80. The experiments described were performed on the hES H9 cell line.

During quinpirole application, a reversible shift of –5.6±1.8 mV was measured when the membrane potential was kept at about –70 mV (supplementary material Fig. S10C), as expected for D2-mediated GIRK channel activation. hiPS cell-derived neurons were also post-marked with biocytin and for CTIP2 (supplementary material Fig. S10D-F).

Altogether, these data indicate that a large proportion of hES/iPS cell-derived MSNs are able to generate single or repetitive action potentials, to develop a functional GABAergic synaptic network that is sensitive to GABA and dopamine stimulation, and show GABAergic spontaneous postsynaptic activity at very low frequency.

Sustained survival and differentiation of grafted hPS cell-derived striatal precursors *in vivo* leads to DARPP-32$^+$ neurons

To assess the viability and differentiation potential of the cells *in vivo*, 5×10^5 day-38 differentiated hES cells were grafted into the striatum of quinolinic acid (QA)-lesioned rats (Fig. 6A,B). Tissue was harvested at 3, 6 and 9 weeks post-transplantation. Immunohistochemical analysis indicated good graft survival at each time point (Fig. 6C-E). No SOX1$^+$ progenitors were detected, and at 6 weeks the grafted striatal progenitors maintained *in vivo* the correct OTX2$^+$ and FOXG1$^+$ identity acquired *in vitro* (supplementary material Fig. S11A-C). Although all grafts were completely devoid of still-pluripotent OCT4$^+$ cells and of signs of teratoma, they continued to exhibit some proliferative potential at 3 weeks, as indicated by positive Ki-67 staining, which did, however, decrease over time (supplementary material Fig. S11D). This trend was also observed for the nestin$^+$ cells (supplementary material Fig. S11D). Importantly, dense fields of MAP2ab$^+$ neurons (Fig. 6F) and elaborated βIII-tubulin$^+$ neurites were present starting at 6 weeks (Fig. 6G), and increased at 9 weeks (supplementary material Fig. S11D). Whereas at 3 weeks no striatal markers were expressed, by 9 weeks post-transplant extensive FOXP1 and FOXP2 staining was evident (Fig. 6H,I; supplementary material Fig. S11D) and DARPP-32 expression was observed, which derived from the grafted cells as demonstrated by co-immunostaining for human nuclei (Fig. 6J,K). FOXP1, FOXP2 and human nuclei immunodetections were performed on serial sections (not shown). This result demonstrated a progressive *in vivo* maturation of the grafted cells toward an MSN fate. Furthermore, projection of nestin$^+$ fibers into the intact striatum suggests integration of the grafts into the host tissue (supplementary material Fig. S11E).

In comparison to a lesion-only control cohort, transplanted rats demonstrated a clear reduction in apomorphine-induced rotational performance. This graft-derived reduction in drug-induced turning was evident from as early as 3 weeks post-graft, at which point grafted rats had reduced from almost 200 ipsilateral turns to fewer than 100 turns per 60-minute session (Fig. 6L). We examined whether the grafted neurons were able to functionally mature and integrate into the host brain. We transplanted hES cell-derived GFP$^+$ striatal precursors *in utero* into E16.5 rat fetuses and recorded from grafted neurons starting from P20 (supplementary material Fig. S12A). Electrophysiology was performed on transplanted brain slices and infrared and epifluorescence videomicroscopy were used to visualize the cell somata of the grafted neurons. Two out of eight cells examined showed clear and complete neuronal differentiation, whereas the others were only partially differentiated. The differentiated neurons showed a mean Na^+ current peak of 4684 pA and the ability to generate a repetitive firing of action potentials (supplementary material Fig. S12B,D). Furthermore, the capability to integrate into the synaptic network was confirmed by the presence of functional synapses, as PSCs were recorded. Owing to the PSC potential for reversal, we concluded that these cells expressed functional glutamatergic synapses (supplementary material Fig. S12D).

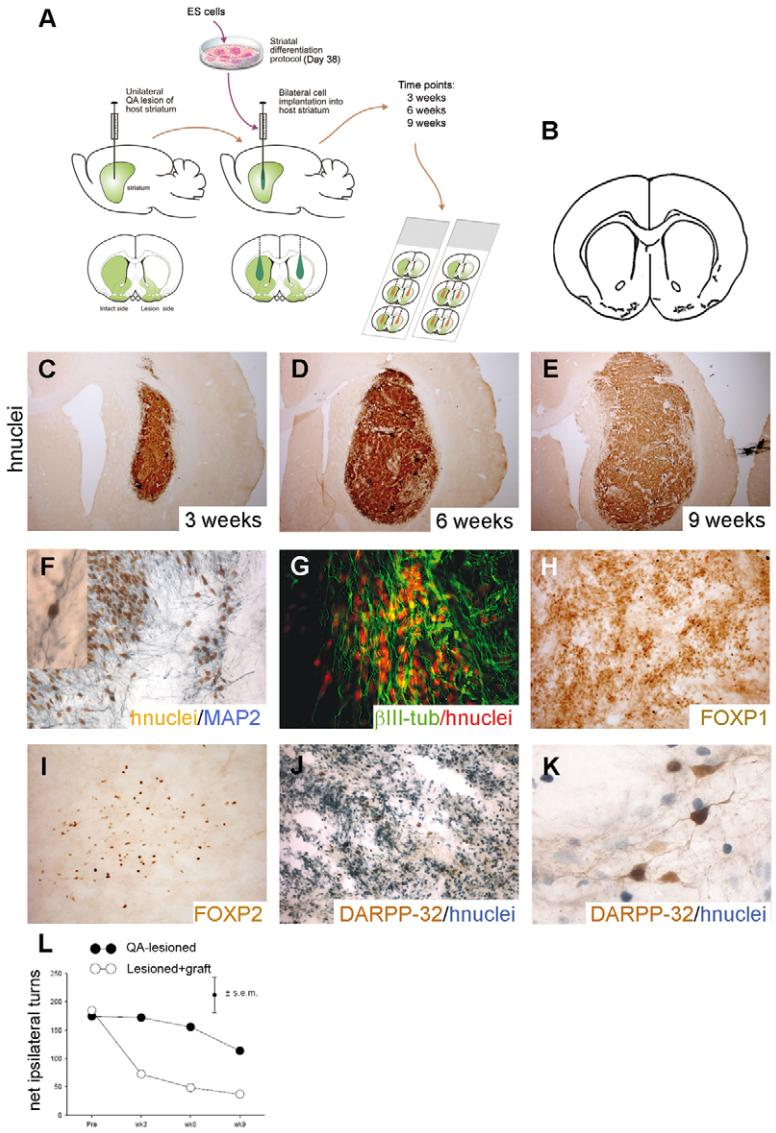

Fig. 6. Assessing the survival and differentiation capacities of *in vitro*-differentiated hES cells after transplantation into rat striatum. (**A**) The transplantation protocol. (**B**) Schematic representation of a coronal section of rat striatum (+0.70 mm from the bregma) showing the region that is lesioned, transplanted and analyzed in the following images by immunohistochemistry. (**C-E**) Graft stained for human nuclei (hnuclei) in the rat striatum at 3, 6 and 9 weeks post-transplantation. (**F-I**) Staining for MAP2ab, FOXP1, FOXP2 (F,H,I), and double labeling of human nuclei with βIII-tubulin (G). (**J**,**K**) Co-staining for DARPP-32 and human nuclei at 9 weeks post-grafting. DARPP-32^{+} neurons/graft, 2145.6±151.05 (mean ± s.d.); total immunopositive for human nuclei, 4×10^{6}/graft. (**L**) Apomorphine-induced rotation test at 3, 6 and 9 weeks after transplantation. Data were analyzed by two-factor ANOVA with repeated measures on tests. The groups × tests effect was highly significant [$F(3,42)=6.34$, $P<0.001$]. Pairwise comparisons by Sidak's test to correct for separate orthogonal comparisons between the two groups at each of the four time points indicated no difference between groups in the pregraft test [$t(29)=0.25$, non-significant], but significance at the 3- and 6-week post-graft tests (3 weeks, $t=2.43$; 6 weeks, $t=2.60$; both $P<0.05$); the 9-weeks test just falls short of significance ($t=1.96$, $P<0.1$). For lesioned+graft, $n=9$ rats, with three for each time point; for lesion-only animals, $n=13$ rats. Original magnifications: 1.6× in C-E; 20× in J; 40× in F-I,K. The experiments described were performed on the hES H9 cell line.

These results clearly demonstrate that transplanted neurons functionally connect with other neurons and that they have the potential to form synaptic networks.

DISCUSSION

By applying the developmental principles that orchestrate ventral telencephalic determination, we successfully recapitulated the process of striatal neurogenesis and instructed hPS cells toward region- and transmitter-specific striatal MSNs. Our three-step method employs a monolayer, feeder-free differentiation paradigm that begins with neuroectodermal specialization of hPS cells via BMP/TGFβ pathway inhibition (Chambers et al., 2009). The crucial neural-inducing activity of noggin has been demonstrated in *Xenopus* (Hemmati-Brivanlou et al., 1994; Sasai et al., 1994; Smith and Harland, 1992), mammals (Valenzuela et al., 1995) and hPS cells (Chambers et al., 2009; Itsykson et al., 2005; Kriks et al., 2011; Shi et al., 2012). Emerging neuroepithelial cells first acquire a rostral phenotype during early development (Stern, 2001), as supported in amphibians by the widely accepted two-signal model proposed by Nieuwkoop (Nieuwkoop, 1952). Consistently, neural progeny differentiated from ES cells first exhibit an anterior phenotype (Pankratz et al., 2007; Watanabe et al., 2005; Gaspard et al., 2008) and then neural progenitors become caudalized. By applying anti-caudalizing signals to block WNT and nodal, telencephalic identity can be maintained (Watanabe et al., 2005).

In the present study, we confirmed that hPS cells efficiently become committed to an anterior fate as demonstrated by the expression of several transcription factors, including OTX2, *SIX3*, *OTX1* and FOXG1. Subpallial determination largely depends on SHH activity (Chiang et al., 1996; Fuccillo et al., 2004; Kohtz et al., 1998; Shimamura and Rubenstein, 1997; Xu et al., 2010), and exogenous SHH drives mouse ES cell differentiation toward a subpallial fate (Danjo et al., 2011). Ventral specification in hES cells requires coordinated WNT inhibition and SHH activation (Li et al., 2009). We patterned hPS cells by means of SHH, combined with DKK1. We used the same SHH concentration as Ma et al. (Ma et al., 2012). However, their protocol is based on aggregation/suspension/plating phases to generate presumptive striatal progenitors and DARPP-32^{+} neurons, the described properties of which do not reveal an authentic MSN character. For example, CTIP2 or GSX2 presence was not analyzed, no suprathreshold repetitive firing or GABA/dopamine neuromodulation was shown, and only 2% of the total cells

surviving after transplantation were CALB1/GABA co-labeled, despite of the high percentage of neurons described as DARPP-32$^+$.

In our terminal differentiation phase, committed cells expressing classical LGE determinants such as GSX2, CTIP2, FOXP1, FOXP2 and *ISL1* (other potential markers were identified by our transcriptome analysis) generated 51% MAP2ab$^+$ neurons, 78% of these being GABAergic. MSN identity was demonstrated using a panel of further markers, including DARPP-32, CALB1, GAD65/67, GABA and *ARPP21*. In addition, the obtained neurons expressed dopamine receptor and adenosine receptor, and 74% of the neurons showed electrophysiological properties consistent with a GABAergic MSN phenotype, as demonstrated by repetitive firing, GABAergic inhibitory sPSCs and response to dopamine neuromodulation. The striatal neurons generated were also able to functionally mature after transplantation into the rat brain and synaptically integrate with host neurons.

To our knowledge, this is the first protocol for directed differentiation of hPS cells into fully characterized MSNs that combines well-defined inductive and patterning molecules in monolayer with a variety of transcription factors to mark the progression toward terminal differentiation. We believe that an exhaustive characterization of the developmental processes is a prerequisite for developing a suitable platform for mechanistic studies and drug screening approaches. We also report, for the first time, a global gene expression profiling in hPS cell-derived striatal cultures. In particular, our unsupervised cluster analysis of the data obtained from the *in vitro*-differentiated cell populations and human fetal samples revealed substantial consistency in the signatures between the groups. The GO classes that emerged from our *in vitro* analysis share a number of categories, such as 'forebrain development', 'cell morphogenesis involved in neuron differentiation' and 'neuron projection morphogenesis', with those obtained in a recent analysis of human brain transcriptome dynamics (Kang et al., 2011). We conclude that the transcriptional changes that we observed during our protocol share similarities with those that occur during human forebrain development.

In this study, we also explored the transplantation of hES cell-derived striatal precursors into the rat QA-lesioned HD model. The results indicated excellent cell survival and extensive axonal projections, suggesting integration of the donor cells into the neuronal network of the host brain. Although transplanted cells integrated and were able to reduce the motor asymmetry in the QA-lesioned model, longer term studies are needed to assess circuit reconstruction and behavioral recovery.

In conclusion, we propose that *in vitro*-generated functional striatal neurons provide a unique experimental paradigm with which to study human neurodevelopment of MSNs. Application of this protocol to HD patient-specific iPS cells (Zhang et al., 2010; Camnasio et al., 2012; The HD iPSC Consortium, 2012) might also contribute to characterization of the specific neuronal population that is affected in HD and help generate a patient/mutation-specific disease model for drug discovery approaches.

Acknowledgements
We thank Federica Poletti for help with cell culture; Kenneth Campbell for providing anti-GSX2 antibody; Elisabetta Cesana for help with electrophysiological analysis; Cecilia Laterza for support in microarray analysis; Lorenzo Magrassi for assistance with *in utero* transplantation; and Outi Hovatta for providing the HS401 cell line. H9 was obtained from Wicell. We also thank the families of HD patients for their continuous support.

Funding
The research leading to these results has received funding from NeuroStemcell, European Union Seventh Framework Programme grant agreement no. 222943, partially from the Ministero dell'Istruzione dell'Università e della Ricerca [MIUR, 2008JKSHKN] and from Cure Huntington's Disease Initiative (CHDI) [ID: A-4529] to E.C., and by Fondo per gli Investimenti della Ricerca di Base [FIRB, RBFR10A01S] to M.O.; A.F. was supported by a Marie Curie fellowship. We acknowledge the important contribution of Tavola Valdese (2007-2010) and the support of Unicredit Banca S.p.A. (Italy).

Competing interests statement
The authors declare no competing financial interests.

Supplementary material
Supplementary material available online at
http://dev.biologists.org/lookup/suppl/doi:10.1242/dev.084608/-/DC1

References

Appolloni, I., Calzolari, F., Corte, G., Perris, R. and Malatesta, P. (2008). Six3 controls the neural progenitor status in the murine CNS. *Cereb. Cortex* **18**, 553-562.
Arlotta, P., Molyneaux, B. J., Jabaudon, D., Yoshida, Y. and Macklis, J. D. (2008). Ctip2 controls the differentiation of medium spiny neurons and the establishment of the cellular architecture of the striatum. *J. Neurosci.* **28**, 622-632.
Aubry, L., Bugi, A., Lefort, N., Rousseau, F., Peschanski, M. and Perrier, A. L. (2008). Striatal progenitors derived from human ES cells mature into DARPP32 neurons in vitro and in quinolinic acid-lesioned rats. *Proc. Natl. Acad. Sci. USA* **105**, 16707-16712.
Beaulieu, J. M. and Gainetdinov, R. R. (2011). The physiology, signaling, and pharmacology of dopamine receptors. *Pharmacol. Rev.* **63**, 182-217.
Camnasio, S., Carri, A. D., Lombardo, A., Grad, I., Mariotti, C., Castucci, A., Rozell, B., Riso, P. L., Castiglioni, V., Zuccato, C. et al. (2012). The first reported generation of several induced pluripotent stem cell lines from homozygous and heterozygous Huntington's disease patients demonstrates mutation related enhanced lysosomal activity. *Neurobiol. Dis.* **46**, 41-51.
Campbell, K. (2003). Dorsal-ventral patterning in the mammalian telencephalon. *Curr. Opin. Neurobiol.* **13**, 50-56.
Chambers, S. M., Fasano, C. A., Papapetrou, E. P., Tomishima, M., Sadelain, M. and Studer, L. (2009). Highly efficient neural conversion of human ES and iPS cells by dual inhibition of SMAD signaling. *Nat. Biotechnol.* **27**, 275-280.
Chiang, C., Litingtung, Y., Lee, E., Young, K. E., Corden, J. L., Westphal, H. and Beachy, P. A. (1996). Cyclopia and defective axial patterning in mice lacking Sonic hedgehog gene function. *Nature* **383**, 407-413.
Danjo, T., Eiraku, M., Muguruma, K., Watanabe, K., Kawada, M., Yanagawa, Y., Rubenstein, J. L. and Sasai, Y. (2011). Subregional specification of embryonic stem cell-derived ventral telencephalic tissues by timed and combinatory treatment with extrinsic signals. *J. Neurosci.* **31**, 1919-1933.
Deacon, T. W., Pakzaban, P. and Isacson, O. (1994). The lateral ganglionic eminence is the origin of cells committed to striatal phenotypes: neural transplantation and developmental evidence. *Brain Res.* **668**, 211-219.
Elkabetz, Y., Panagiotakos, G., Al Shamy, G., Socci, N. D., Tabar, V. and Studer, L. (2008). Human ES cell-derived neural rosettes reveal a functionally distinct early neural stem cell stage. *Genes Dev.* **22**, 152-165.
Ericson, J., Muhr, J., Jessell, T. M. and Edlund, T. (1995). Sonic hedgehog: a common signal for ventral patterning along the rostrocaudal axis of the neural tube. *Int. J. Dev. Biol.* **39**, 809-816.
Ericsson, J., Silberberg, G., Robertson, B., Wikstrom, M. A. and Grillner, S. (2011). Striatal cellular properties conserved from lampreys to mammals. *J. Physiol.* **589**, 2979-2992.
Fuccillo, M., Rallu, M., McMahon, A. P. and Fishell, G. (2004). Temporal requirement for hedgehog signaling in ventral telencephalic patterning. *Development* **131**, 5031-5040.
Gaspard, N. and Vanderhaeghen, P. (2010). From stem cells to neural networks: recent advances and perspectives for neurodevelopmental disorders. *Dev. Med. Child Neurol.* **53**, 13-17.
Gaspard, N., Bouschet, T., Hourez, R., Dimidschstein, J., Naeije, G., van den Ameele, J., Espuny-Camacho, I., Herpoel, A., Passante, L., Schiffmann, S. N. et al. (2008). An intrinsic mechanism of corticogenesis from embryonic stem cells. *Nature* **455**, 351-357.
Girault, J. A., Walaas, S. I., Hemmings, H. C., Jr and Greengard, P. (1990). ARPP-21, a cAMP-regulated phosphoprotein enriched in dopamine-innervated brain regions: tissue distribution and regulation of phosphorylation in rat brain. *Neuroscience* **37**, 317-325.
Hemmati-Brivanlou, A., Kelly, O. G. and Melton, D. A. (1994). Follistatin, an antagonist of activin, is expressed in the Spemann organizer and displays direct neuralizing activity. *Cell* **77**, 283-295.
Itsykson, P., Ilouz, N., Turetsky, T., Goldstein, R. S., Pera, M. F., Fishbein, I., Segal, M. and Reubinoff, B. E. (2005). Derivation of neural precursors from human embryonic stem cells in the presence of noggin. *Mol. Cell. Neurosci.* **30**, 24-36.

Jiang, Z. G. and North, R. A. (1991). Membrane properties and synaptic responses of rat striatal neurones in vitro. *J. Physiol.* **443**, 533-553.
Kang, H. J., Kawasawa, Y. I., Cheng, F., Zhu, Y., Xu, X., Li, M., Sousa, A. M., Pletikos, M., Meyer, K. A., Sedmak, G. et al. (2011). Spatio-temporal transcriptome of the human brain. *Nature* **478**, 483-489.
Koch, P., Opitz, T., Steinbeck, J. A., Ladewig, J. and Brustle, O. (2009). A rosette-type, self-renewing human ES cell-derived neural stem cell with potential for in vitro instruction and synaptic integration. *Proc. Natl. Acad. Sci. USA* **106**, 3225-3230.
Kohtz, J. D., Baker, D. P., Corte, G. and Fishell, G. (1998). Regionalization within the mammalian telencephalon is mediated by changes in responsiveness to sonic hedgehog. *Development* **125**, 5079-5089.
Kreitzer, A. C. (2009). Physiology and pharmacology of striatal neurons. *Annu. Rev. Neurosci.* **32**, 127-147.
Kriks, S., Shim, J. W., Piao, J., Ganat, Y. M., Wakeman, D. R., Xie, Z., Carrillo-Reid, L., Auyeung, G., Antonacci, C., Buch, A. et al. (2011). Dopamine neurons derived from human ES cells efficiently engraft in animal models of Parkinson's disease. *Nature* **480**, 547-551.
Kuzhikandathil, E. V., Yu, W. and Oxford, G. S. (1998). Human dopamine D3 and D2L receptors couple to inward rectifier potassium channels in mammalian cell lines. *Mol. Cell. Neurosci.* **12**, 390-402.
Lavine, N., Ethier, N., Oak, J. N., Pei, L., Liu, F., Trieu, P., Rebois, R. V., Bouvier, M., Hebert, T. E. and Van Tol, H. H. (2002). G protein-coupled receptors form stable complexes with inwardly rectifying potassium channels and adenylyl cyclase. *J. Biol. Chem.* **277**, 46010-46019.
Li, X. J., Zhang, X., Johnson, M. A., Wang, Z. B., Lavaute, T. and Zhang, S. C. (2009). Coordination of sonic hedgehog and Wnt signaling determines ventral and dorsal telencephalic neuron types from human embryonic stem cells. *Development* **136**, 4055-4063.
Liu, H. and Zhang, S. C. (2011). Specification of neuronal and glial subtypes from human pluripotent stem cells. *Cell. Mol. Life Sci.* **68**, 3995-4008.
Lupo, G., Harris, W. A. and Lewis, K. E. (2006). Mechanisms of ventral patterning in the vertebrate nervous system. *Nat. Rev. Neurosci.* **7**, 103-114.
Ma, L., Hu, B., Liu, Y., Vermilyea, S. C., Liu, H., Gao, L., Sun, Y., Zhang, X. and Zhang, S. C. (2012). Human embryonic stem cell-derived GABA neurons correct locomotion deficits in quinolinic acid-lesioned mice. *Cell Stem Cell* **10**, 455-464.
Manuel, M., Martynoga, B., Yu, T., West, J. D., Mason, J. O. and Price, D. J. (2010). The transcription factor Foxg1 regulates the competence of telencephalic cells to adopt subpallial fates in mice. *Development* **137**, 487-497.
Marullo, M., Zuccato, C., Mariotti, C., Lahiri, N., Tabrizi, S. J., Di Donato, S. and Cattaneo, E. (2010). Expressed Alu repeats as a novel, reliable tool for normalization of real-time quantitative RT-PCR data. *Genome Biol.* **11**, R9.
Mauri, M., Lentini, D., Gravati, M., Foudah, D., Biella, G., Costa, B., Toselli, M., Parenti, M. and Coco, S. (2012). Mesenchymal stem cells enhance GABAergic transmission in co-cultured hippocampal neurons. *Mol. Cell. Neurosci.* **49**, 395-405.
Nat, R. and Dechant, G. (2011). Milestones of directed differentiation of mouse and human embryonic stem cells into telencephalic neurons based on neural development in vivo. *Stem Cells Dev.* **20**, 947-958.
Nieuwkoop, P. D. (1952). Activation and organization of the central nervous system in amphibians. *J. Exp. Zool.* **120**, 33-81.
Nisenbaum, E. S., Wilson, C. J., Foehring, R. C. and Surmeier, D. J. (1996). Isolation and characterization of a persistent potassium current in neostriatal neurons. *J. Neurophysiol.* **76**, 1180-1194.
Nogales-Cadenas, R., Carmona-Saez, P., Vazquez, M., Vicente, C., Yang, X., Tirado, F., Carazo, J. M. and Pascual-Montano, A. (2009). GeneCodis: interpreting gene lists through enrichment analysis and integration of diverse biological information. *Nucleic Acids Res.* **37**, W317-W322.
Olsson, M., Campbell, K., Wictorin, K. and Bjorklund, A. (1995). Projection neurons in fetal striatal transplants are predominantly derived from the lateral ganglionic eminence. *Neuroscience* **69**, 1169-1182.
Onorati, M., Binetti, M., Conti, L., Camnasio, S., Calabrese, G., Albieri, I., Di Febo, F., Toselli, M., Biella, G., Martynoga, B. et al. (2011). Preservation of positional identity in fetus-derived neural stem (NS) cells from different mouse central nervous system compartments. *Cell. Mol. Life Sci.* **68**, 1769-1783.
Ouimet, C. C., Miller, P. E., Hemmings, H. C., Jr, Walaas, S. I. and Greengard, P. (1984). DARPP-32, a dopamine- and adenosine 3′:5′-monophosphate-regulated phosphoprotein enriched in dopamine-innervated brain regions. III. Immunocytochemical localization. *J. Neurosci.* **4**, 111-124.
Ouimet, C. C., Langley-Gullion, K. C. and Greengard, P. (1998). Quantitative immunocytochemistry of DARPP-32-expressing neurons in the rat caudatoputamen. *Brain Res.* **808**, 8-12.
Pankratz, M. T., Li, X. J., Lavaute, T. M., Lyons, E. A., Chen, X. and Zhang, S. C. (2007). Directed neural differentiation of human embryonic stem cells via an obligated primitive anterior stage. *Stem Cells* **25**, 1511-1520.
Saeed, A. I., Bhagabati, N. K., Braisted, J. C., Liang, W., Sharov, V., Howe, E. A., Li, J., Thiagarajan, M., White, J. A. and Quackenbush, J. (2006). TM4 microarray software suite. *Methods Enzymol.* **411**, 134-193.
Sasai, Y., Lu, B., Steinbeisser, H., Geissert, D., Gont, L. K. and De Robertis, E. M. (1994). Xenopus chordin: a novel dorsalizing factor activated by organizer-specific homeobox genes. *Cell* **79**, 779-790.
Schuurmans, C. and Guillemot, F. (2002). Molecular mechanisms underlying cell fate specification in the developing telencephalon. *Curr. Opin. Neurobiol.* **12**, 26-34.
Shen, W., Hernandez-Lopez, S., Tkatch, T., Held, J. E. and Surmeier, D. J. (2004). Kv1.2-containing K^+ channels regulate subthreshold excitability of striatal medium spiny neurons. *J. Neurophysiol.* **91**, 1337-1349.
Shi, Y., Kirwan, P., Smith, J., Robinson, H. P. and Livesey, F. J. (2012). Human cerebral cortex development from pluripotent stem cells to functional excitatory synapses. *Nat. Neurosci.* **15**, 477-486.
Shimamura, K. and Rubenstein, J. L. (1997). Inductive interactions direct early regionalization of the mouse forebrain. *Development* **124**, 2709-2718.
Smith, W. C. and Harland, R. M. (1992). Expression cloning of noggin, a new dorsalizing factor localized to the Spemann organizer in Xenopus embryos. *Cell* **70**, 829-840.
Smith, Y., Bevan, M. D., Shink, E. and Bolam, J. P. (1998). Microcircuitry of the direct and indirect pathways of the basal ganglia. *Neuroscience* **86**, 353-387.
Smyth, G. K. (2004). Linear models and empirical Bayes methods for assessing differential expression in microarray experiments. *Stat. Appl. Genet. Mol. Biol.* **3**, Article3.
Stern, C. D. (2001). Initial patterning of the central nervous system: how many organizers? *Nat. Rev. Neurosci.* **2**, 92-98.
Surmeier, D. J., Bargas, J. and Kitai, S. T. (1989). Two types of A-current differing in voltage-dependence are expressed by neurons of the rat neostriatum. *Neurosci. Lett.* **103**, 331-337.
Surmeier, D. J., Stefani, A., Foehring, R. C. and Kitai, S. T. (1991). Developmental regulation of a slowly-inactivating potassium conductance in rat neostriatal neurons. *Neurosci. Lett.* **122**, 41-46.
The HD iPSC Consortium (2012). Induced pluripotent stem cells from patients with Huntington's disease show CAG-repeat-expansion-associated phenotypes. *Cell Stem Cell* **11**, 264-278.
Torres, E. M., Dowd, E. and Dunnett, S. B. (2008). Recovery of functional deficits following early donor age ventral mesencephalic grafts in a rat model of Parkinson's disease. *Neuroscience* **154**, 631-640.
Ungerstedt, U. and Arbuthnott, G. W. (1970). Quantitative recording of rotational behavior in rats after 6-hydroxy-dopamine lesions of the nigrostriatal dopamine system. *Brain Res.* **24**, 485-493.
Valenzuela, D. M., Economides, A. N., Rojas, E., Lamb, T. M., Nunez, L., Jones, P., Lp, N. Y., Espinosa, R., 3rd, Brannan, C. I., Gilbert, D. J. et al. (1995). Identification of mammalian noggin and its expression in the adult nervous system. *J. Neurosci.* **15**, 6077-6084.
Wang, H. F. and Liu, F. C. (2001). Developmental restriction of the LIM homeodomain transcription factor Islet-1 expression to cholinergic neurons in the rat striatum. *Neuroscience* **103**, 999-1016.
Watanabe, K., Kamiya, D., Nishiyama, A., Katayama, T., Nozaki, S., Kawasaki, H., Watanabe, Y., Mizuseki, K. and Sasai, Y. (2005). Directed differentiation of telencephalic precursors from embryonic stem cells. *Nat. Neurosci.* **8**, 288-296.
Xu, Q., Guo, L., Moore, H., Waclaw, R. R., Campbell, K. and Anderson, S. A. (2010). Sonic hedgehog signaling confers ventral telencephalic progenitors with distinct cortical interneuron fates. *Neuron* **65**, 328-340.
Zhang, S. C., Wernig, M., Duncan, I. D., Brustle, O. and Thomson, J. A. (2001). In vitro differentiation of transplantable neural precursors from human embryonic stem cells. *Nat. Biotechnol.* **19**, 1129-1133.
Zhang, N., An, M. C., Montoro, D. and Ellerby, L. M. (2010). Characterization of human Huntington's disease cell model from induced pluripotent stem cells. *PLoS Curr.* **2**, RRN1193.
Zhang, X., Huang, C. T., Chen, J., Pankratz, M. T., Xi, J., Li, J., Yang, Y., Lavaute, T. M., Li, X. J., Ayala, M. et al. (2010). Pax6 is a human neuroectoderm cell fate determinant. *Cell Stem Cell* **7**, 90-100.
Zhou, J., Su, P., Li, D., Tsang, S., Duan, E. and Wang, F. (2010). High-efficiency induction of neural conversion in human ESCs and human induced pluripotent stem cells with a single chemical inhibitor of transforming growth factor beta superfamily receptors. *Stem Cells* **28**, 1741-1750.
Zuccato, C., Valenza, M. and Cattaneo, E. (2010). Molecular mechanisms and potential therapeutical targets in Huntington's disease. *Physiol. Rev.* **90**, 905-981.

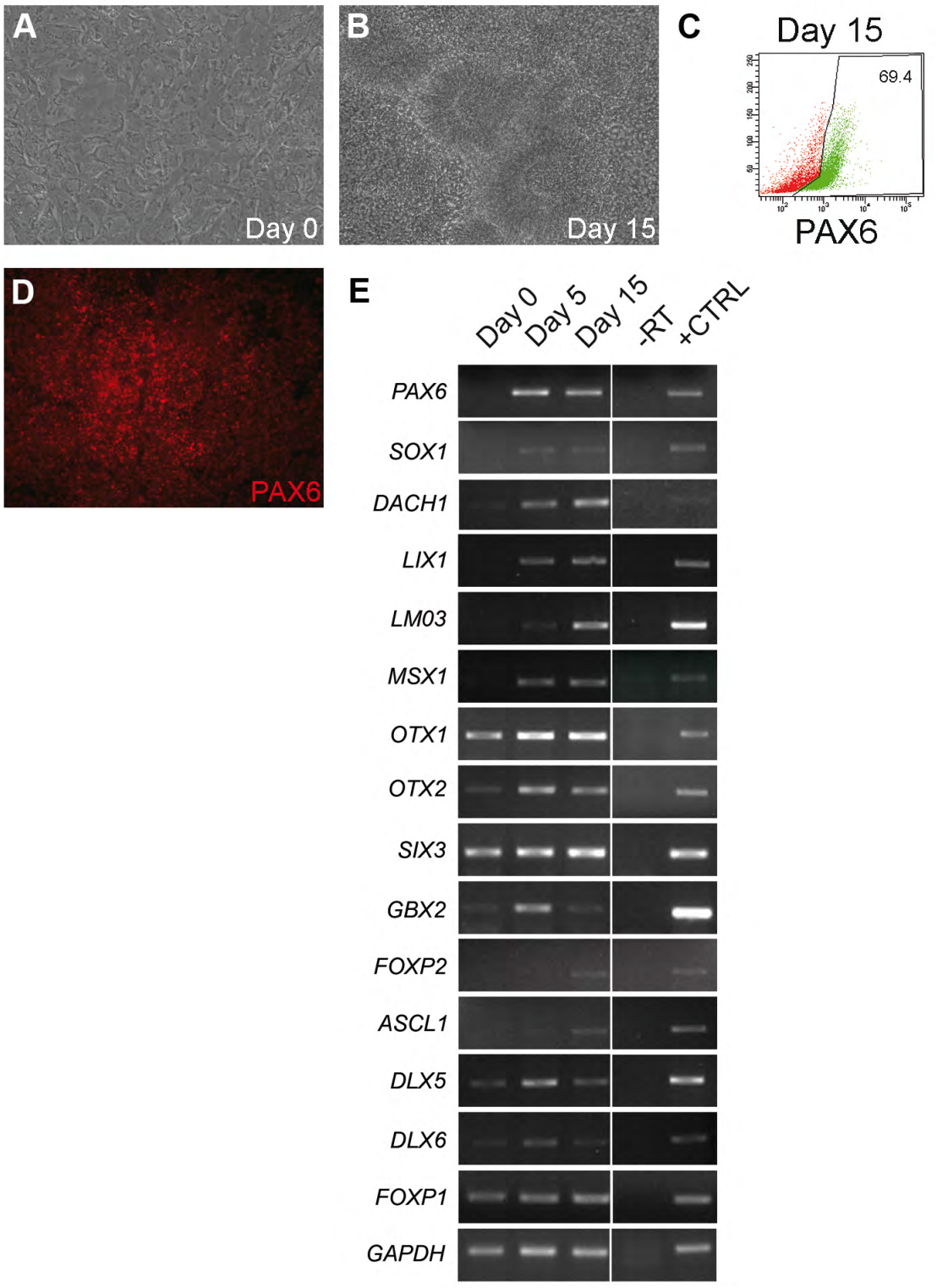

Fig. S1. Neural induction phase in the presence of noggin and SB431542. (**A**,**B**) Live images of cells during neural induction. Rosettes are evident at day 15 (B), as compared with day 0 (A) (original magnification 10×). (**C**) Flow cytometry at day 15 showing that 69.4% of the cells are PAX6^{+}. (**D**) In the presence of the noggin analog LDN-193189, the cells at day 15 express PAX6, similar to the effect of noggin and dorsomorphin exposure. (**E**) RT-PCR analysis for relevant neuroectodermal and regional markers. –RT, control without reverse transcriptase; +CTRL, cDNA from human fetal striatum. The experiments described were performed on hES H9 cell line.

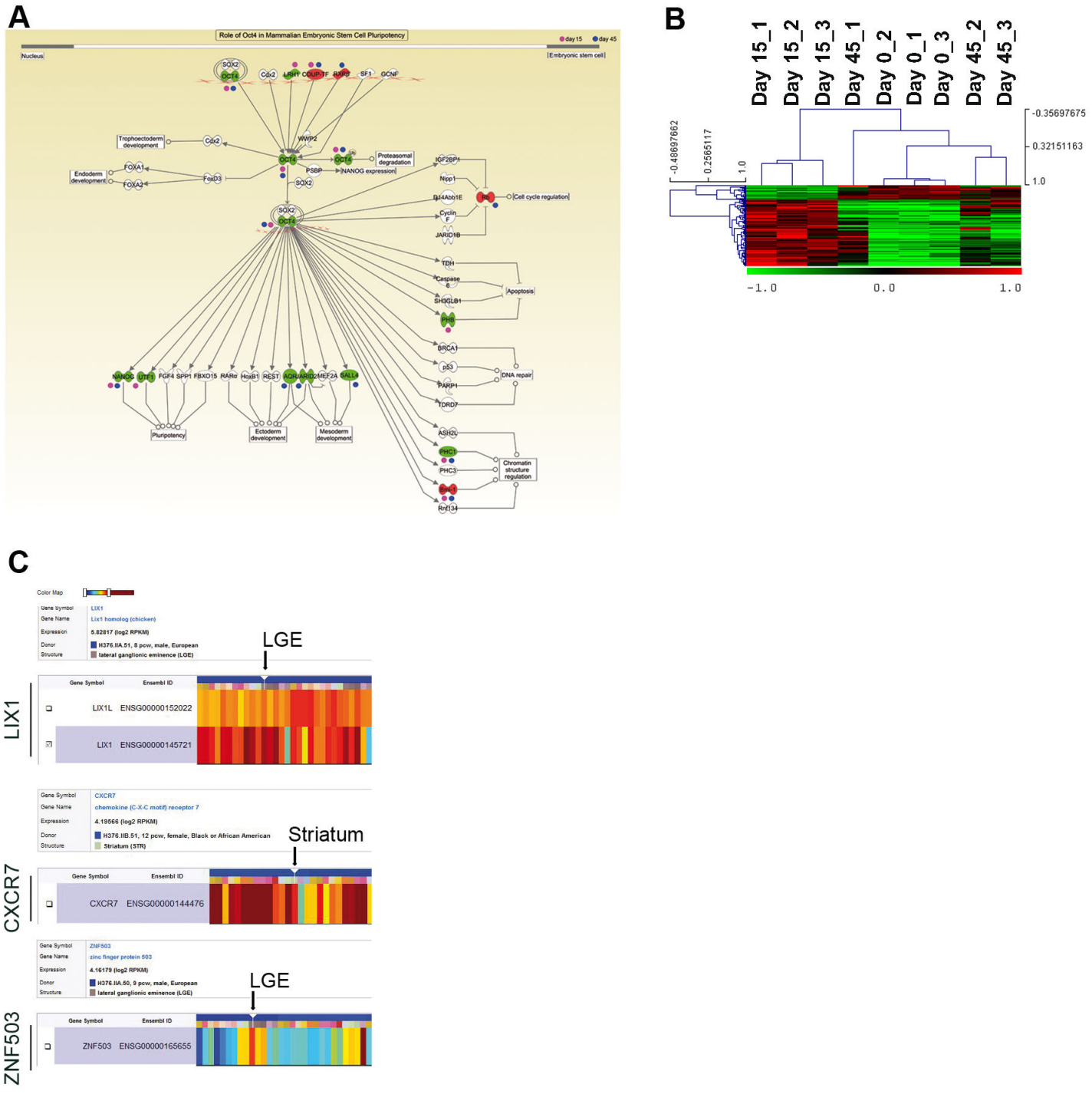

Fig. S2. Genome-wide gene expression analysis of the neural induction phase. (**A**) Ingenuity pathway analysis on day-15 and day-45 transcriptional signatures highlights significant enrichment in the OCT4-regulated pathway. (**B**) Stage-specific subcluster of the day-15 transcriptional signature (three biological replicates for each condition). (**C**) Candidate LGE-specific markers deriving from DEGs in the subcluster were online validated using the Allen human gene expression database (http://human.brain-map.org).

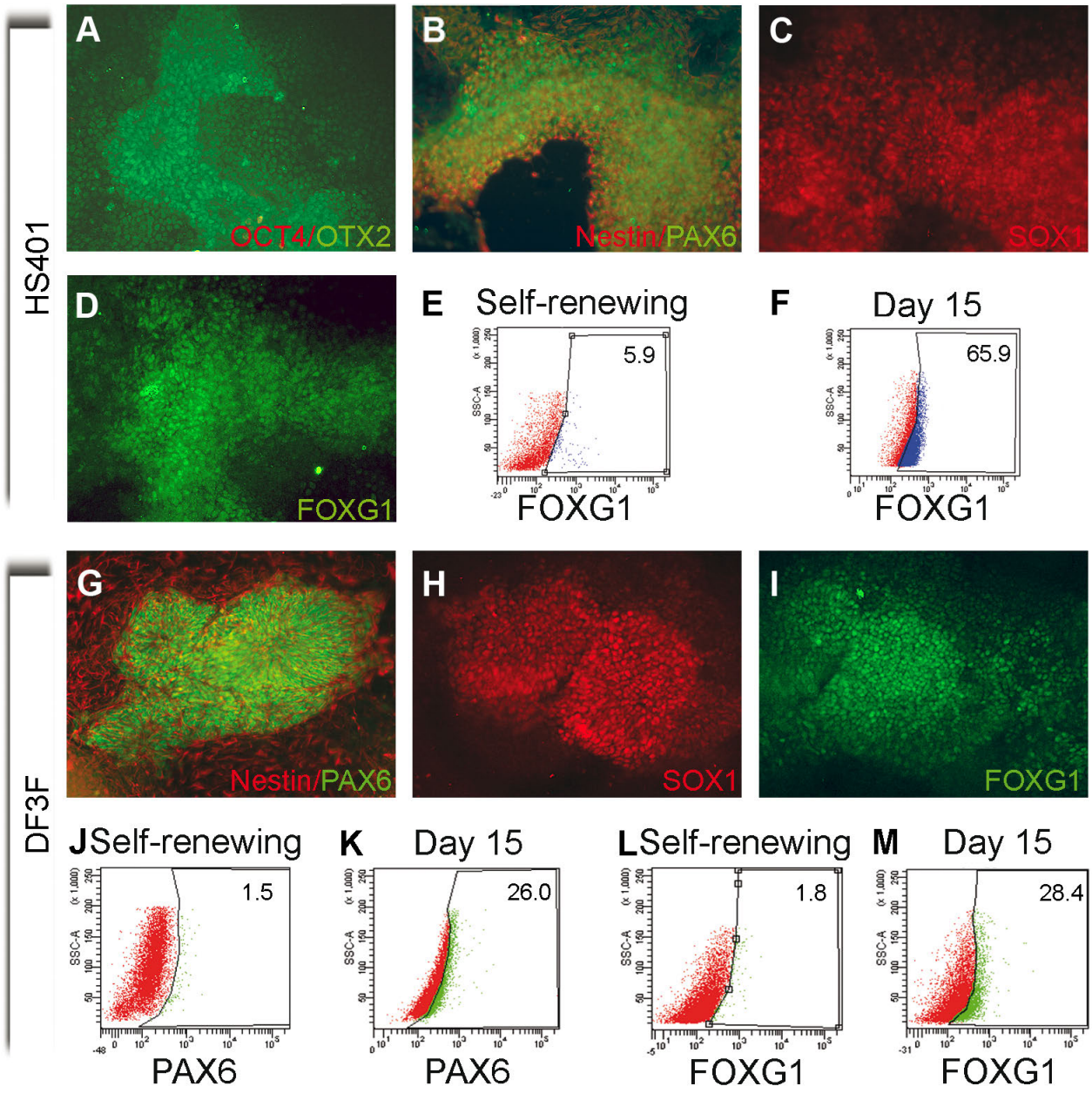

Fig. S3. Application of the neural conversion method to hES and hiPS cell lines leads to the efficient generation of ventral telencephalic progenitors. HS401 hES (A-F) and DF3F hiPS (G-M) cell lines. (**A**) OCT4 and OTX2 staining of HS401 cells at the end of neural induction, day 15. (**B**,**C**) PAX6, nestin and SOX1 are expressed in neuralized cells. (**D**) FOXG1$^+$ cells appear after the neural induction and patterning phase. (**E**,**F**) Flow cytometric analysis on generated neural progenitors. At day 15 of differentiation, 65.9% of the cells expressed FOXG1. (**G**,**H**) The neuroectodermal markers nestin, PAX6 and SOX1 are expressed on day 15 of DF3F differentiation. (**I**) FOXG1 expression revealed the emergence of telencephalic patterned progenitors (original magnification 20×). (**J-M**) Flow cytometric analysis during neural conversion for PAX6 and FOXG1. At day 15, 26% of cells are PAX6$^+$ and 28.4% are FOXG1$^+$.

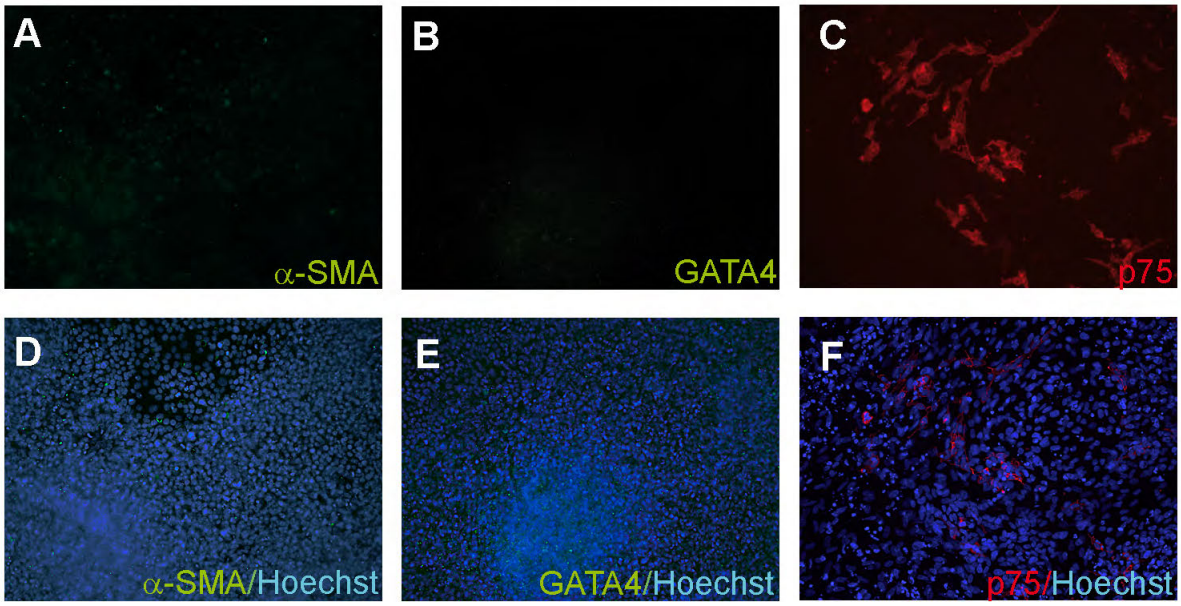

Fig. S4. Treatment with dorsomorphin and SB431542 selectively induces neuroectodermal fate. Lack of the mesodermal (α-SMA) (**A**,**D**) and endodermal (GATA4) (**B**,**E**) markers at day 15 of differentiation. Some cells are positive for the neural crest marker p75 (p75NTR; NGFR – Human Gene Nomenclature Committee) (**C**,**F**) after neural conversion at 15 days of differentiation. The experiments described were performed on hES H9 cell line.

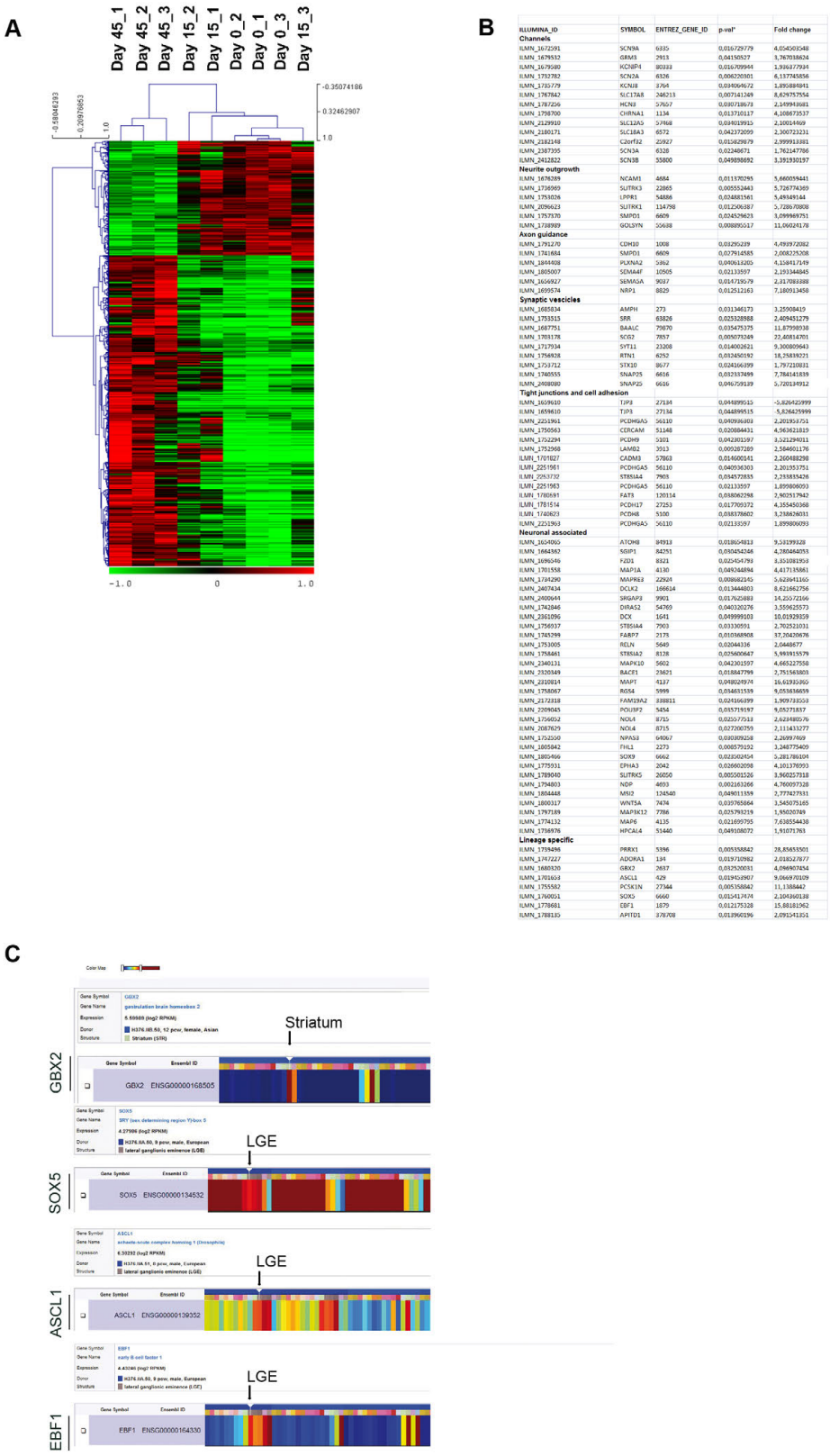

Fig. S5. Genome-wide gene expression analysis of the terminal differentiation phase. (**A**) Stage-specific subcluster of the day-45 transcriptional signature (three biological replicates for each condition). (**B**) Summary including a selected list of day-45-specific differentially expressed transcripts. (**C**) Candidate striatal-specific markers present in the day-45 transcriptional subcluster were online validated using the Allen human gene expression database (http://human.brain-map.org).

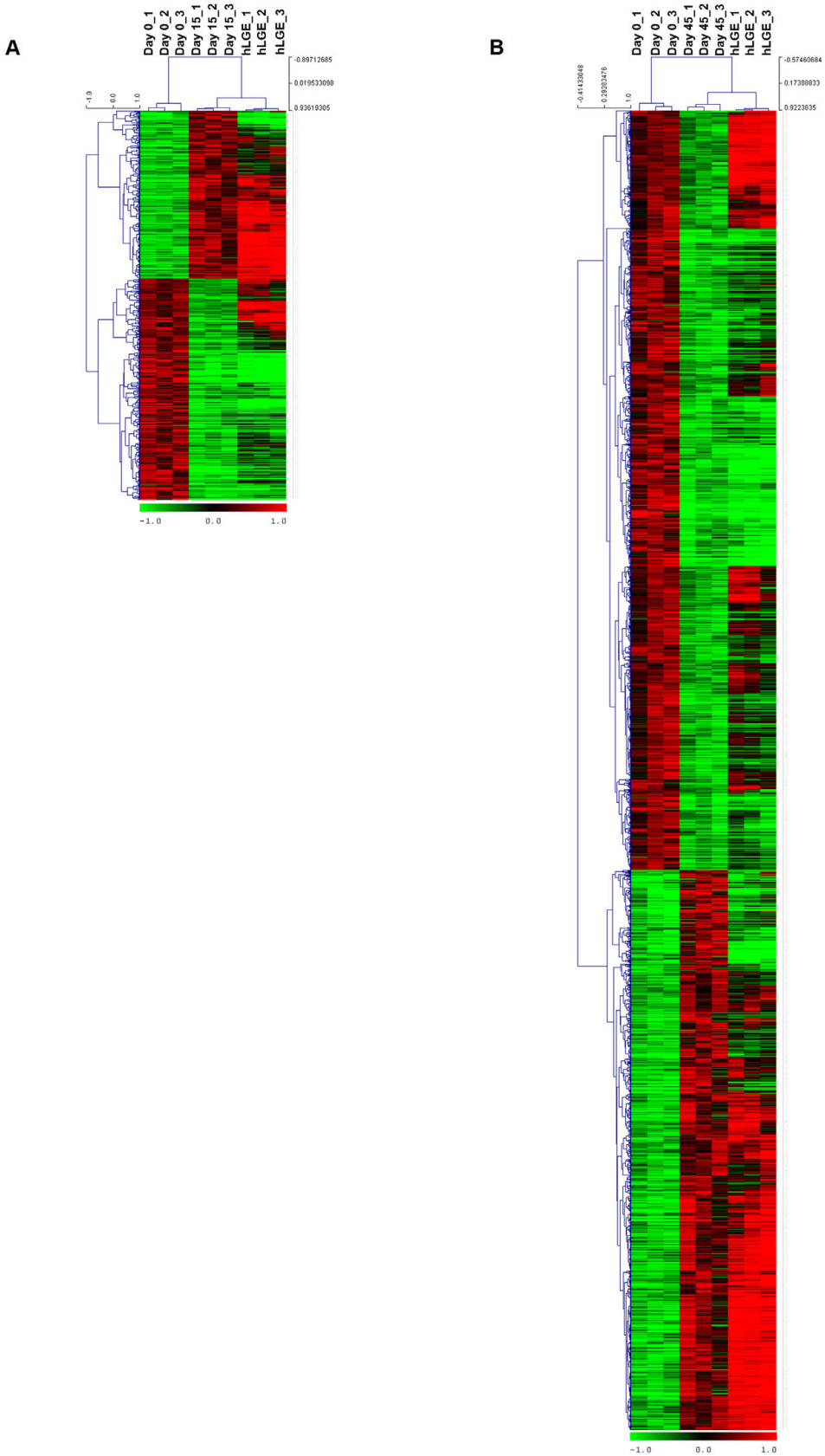

Fig. S7. Neurochemical investigation of neuronal subtypes differentiated from hES cells. (**A**,**B**) Immunofluorescence for MAP2ab, βIII-tubulin, nestin (A) and GFAP (B) at day 80 of differentiation. (**C**) The composition of the total cell population: 51±3% MAP2^{+} cells, *n*=1126 cells; 25±0.03% GFAP^{+} cells, *n*=712 cells; 7±4.9% nestin^{+} cells, *n*=220 cells; 17.3±5.03% nestin/βIII-tubulin double-positive cells, *n*=208 cells. (**D**,**E**) Co-expression of GABA/CTIP2 (D) and CALB1/CTIP2 (E). (**F**,**G**) Analysis of the interneuronal markers neuropeptide Y (NPY) and calretinin (CR) (F) and parvalbumin (PVALB) and somatostatin (SST) (G) at day 80. (**H**) Tyrosine hydroxylase (TH) and 5-hydroxytriptamine (5-HT) immunoreactive neurons at the end of terminal differentiation. (**I**) Immunodetection for vesicular glutamate transporter 1 (VGLUT1). The experiments described were performed on hES H9 cell line.

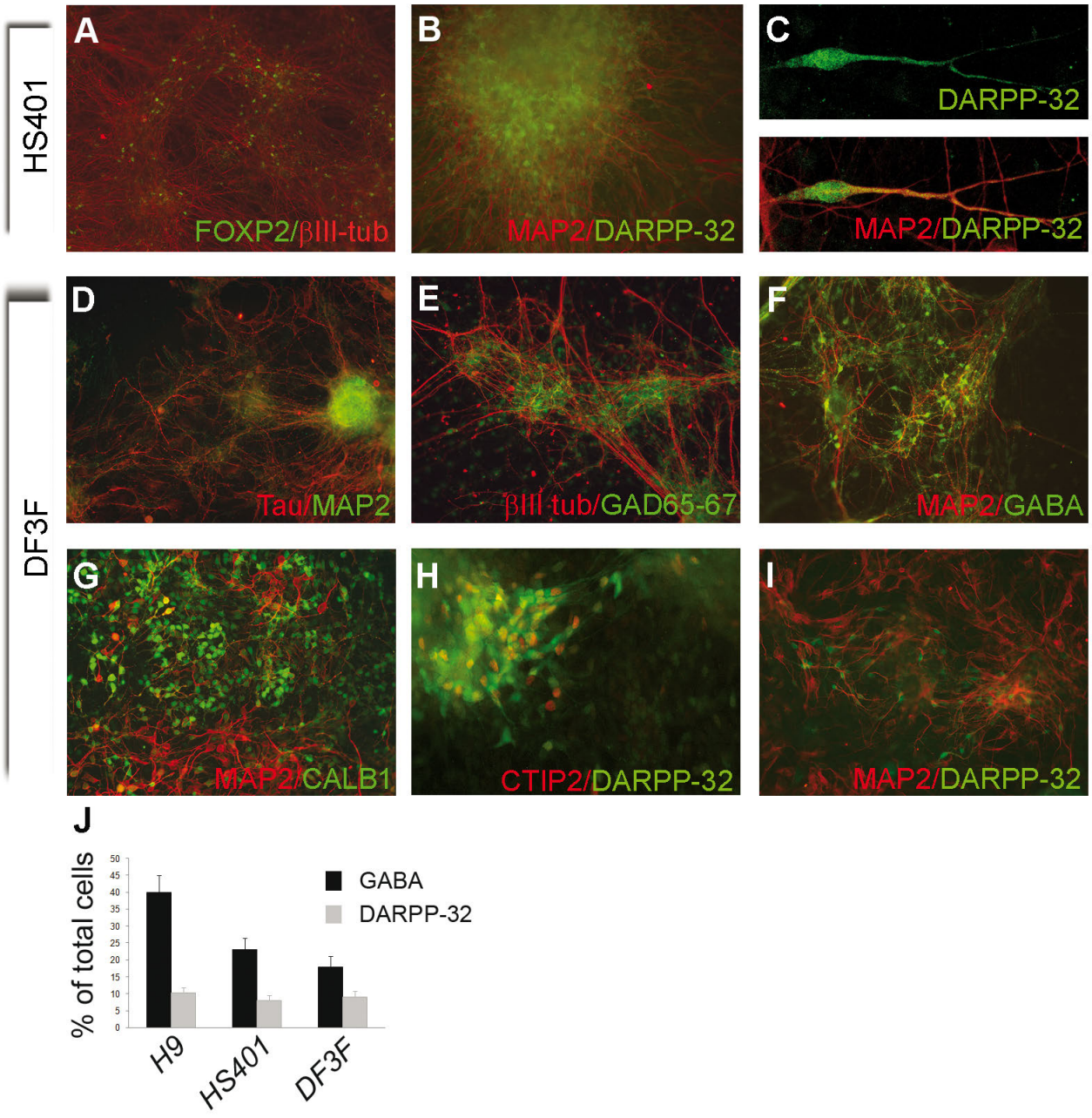

Fig. S8. HS401 and DF3F cells can also be patterned and differentiated to striatal neurons according to the established protocol. (A-C) HS401 cells; (D-I) DF3F cells. (**A**) Immunodetection of FOXP2 in differentiated HS401-derived neurons at day 45. (**B**) After terminal differentiation, 8.1±1% of the cells express DARPP-32 (*n*=1820 cells) (original magnification 20×). (**C**) Confocal analysis revealing the morphology of DARPP-32^{+} neurons (original magnification 40×). (**D-I**) Terminally differentiated DF3F-derived neurons express the mature pan-neuronal markers MAP2ab and TAU (D), the GABAergic markers GAD65/67 (E), GABA (F), calbindin (CALB1) (G), and the striatal markers CTIP2 (H) and DARPP-32 (I) (9.1±1.6% of the total cells, *n*=2145 cells; mean ± s.d.) (original magnification 20×). (**J**) A comparative assessment of the percentage of GABA^{+} and DARPP-32^{+} neurons among H9, HS401 hES cells and DF3F hiPS cell lines. HS401: GABA 23±3%, *n*=2226 cells; DARPP-32 8.1±1%, *n*=1820 cells. DF3F: GABA 17.8±3%, *n*=1153 cells; DARPP-32 9.1±1.6%, *n*=2145 cells (mean ± s.d.).

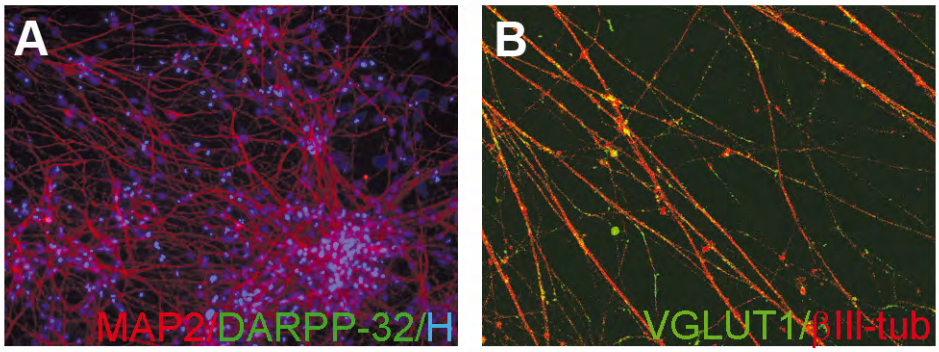

Fig. S9. Neuronal differentiation analysis in the absence of SHH/DKK1 morphogens. At the end of the differentiation the cells do not show positivity for DARPP-32 (**A**), whereas they widely express the glutamatergic marker VGLUT1 (**B**). The experiments described were performed on hES H9 cell line.

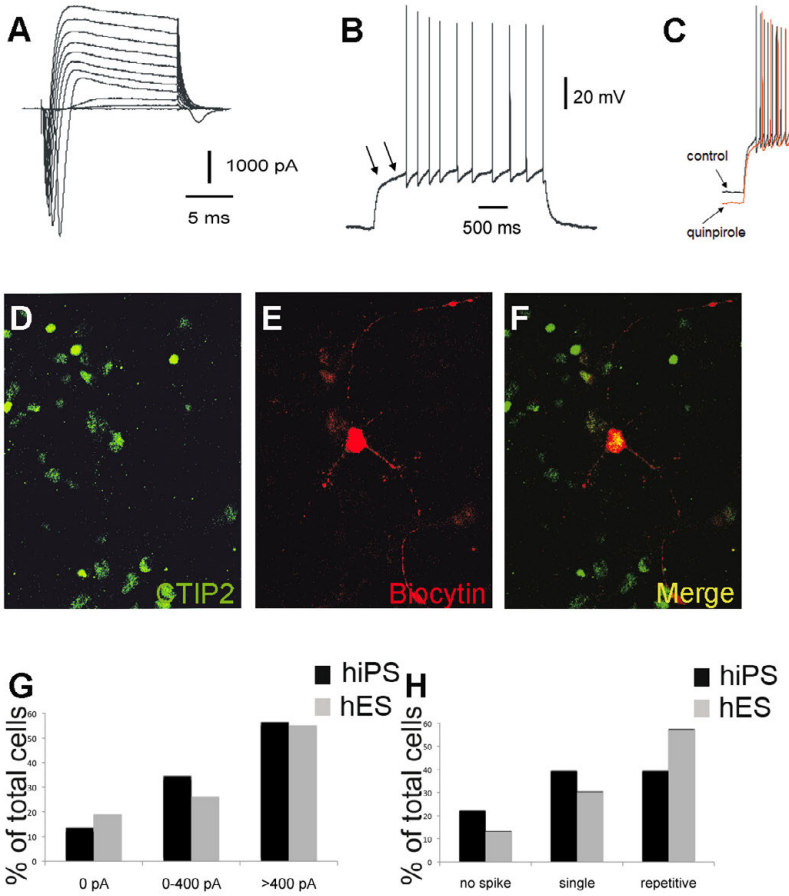

Fig. S10. Electrophysiological properties of fully differentiated hiPS-derived neurons. (**A**) Family of total inward and outward currents elicited at test potentials ranging from –70 to +40 mV from a holding voltage of –90 mV. (**B**) Sample trace obtained in current-clamp configuration showed repetitive firing in a 73-day differentiated neuron when excited with a suprathreshold depolarizing step of current. Note that the onset delay in the generation of the first spike (arrows) is a typical electrophysiological property of mature MSNs. (**C**) The application of quinpirole (5 μM), a D2 agonist, in two out of four cells induced hyperpolarization of the membrane potential. (**D-F**) Confocal image of double labeling of a recorded cell with biocytin and for CTIP2 (original magnification 40×). (**G**) The fraction of cells (hiPS and hES cells) subdivided into three groups according to the amplitude of the Na^+ current peak. hiPS cells: 0 pA, 12% (*n*=2 cells); <400 pA (315±25, mean ± s.e.m.), 33% (*n*=6 cells); >400 pA (–1746±481), 55% (*n*=10 cells). hES cells: 0 pA, 19% (*n*=11 cells); <400 pA (–218±25.00 pA), 26% (*n*=15 cells); >400 pA (–1750±250 pA), 55% (*n*=32 cells). (**H**) The fraction of cells (hiPS and hES cells) subdivided into three groups according to their firing properties. hiPS cell-derived neurons: no spike, 22% (*n*=4 cells); single spike, 39% (*n*=7 cells); repetitive firing, 39% (*n*=7 cells). hES cell-derived neurons: no spike, 13% (*n*=3 cells); single spike, 30% (*n*=7 cells); repetitive firing, 57% (*n*=13 cells). The experiments described were performed on the hiPS DF3F cell line compared with the hES H9 cell line.

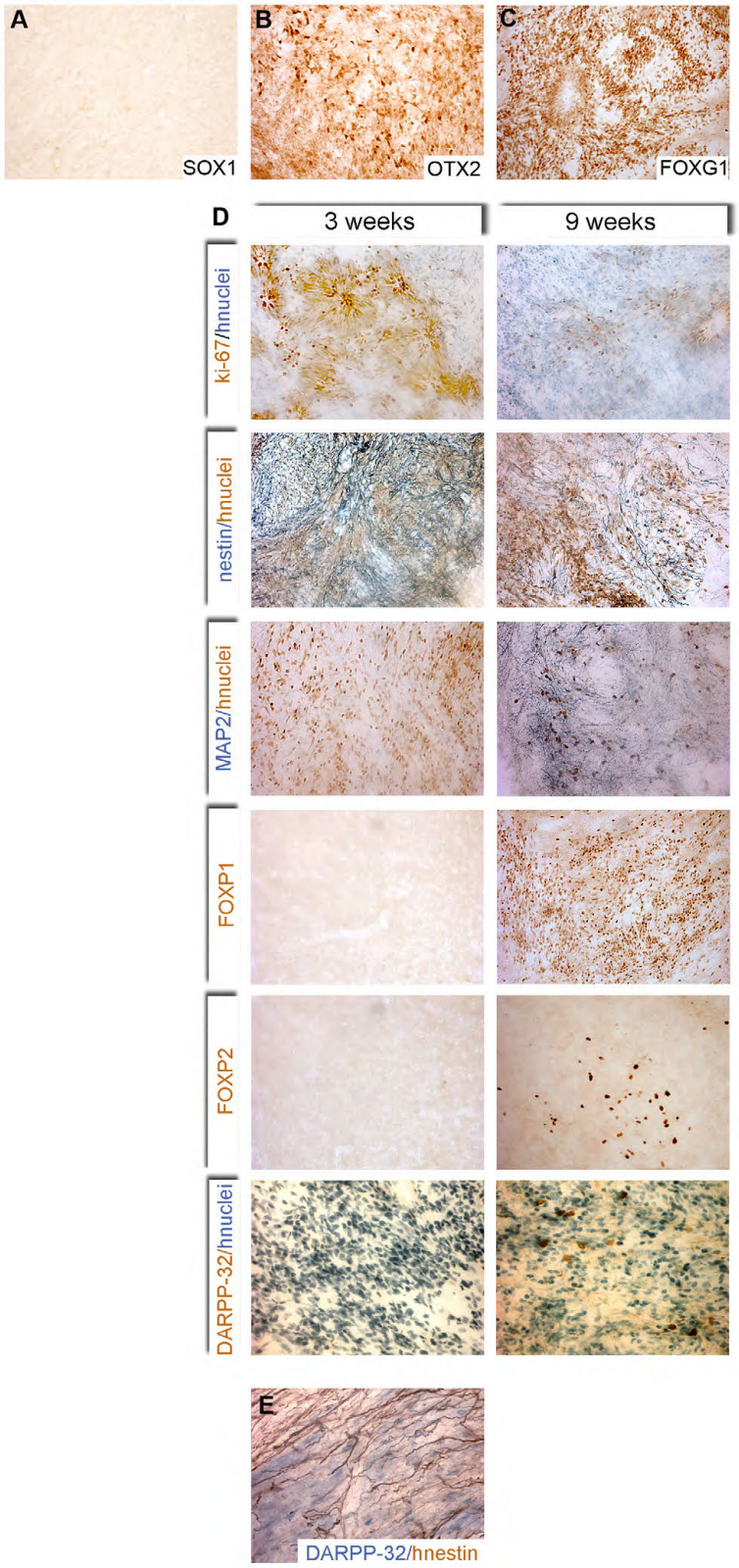

Fig. S11. Characterization of transplanted striatal precursors in striata from HD rats. (**A**) Immunohistochemical staining of a 9-week-old graft reveals no evidence of SOX1 expression. (**B**,**C**) OTX2 and FOXG1 immunostaining. (**D**) Timecourse analysis of proliferating (Ki-67, nestin), differentiated neurons (MAP2ab), and striatal neurons (FOXP1, FOXP2, DARPP-32) throughout the analyzed time points. Ki-67$^+$ cells: at 3 weeks, 56.38±7.72%; at 9 weeks, 22.55±3.02% of the hnuclei$^+$ cells; *n*=3 brains/time point. FOXP1: at 3 weeks, no cells; at 9 weeks, 18.49% of hnuclei$^+$ cells; *n*=1 brain/time point. FOXP2: at 3 weeks, no cells; at 9 weeks, 0.56% of hnuclei$^+$ cells; *n*=1 brain/time point. DARPP-32: at 3 weeks, no cells; at 9 weeks, 0.017±0.002% of hnuclei$^+$ cells; *n*=3 brains/time point. Percentage expressed as mean ± s.e.m. (**E**) Nestin-labeled projections (brown) were evident in the intact DARPP-32$^+$ striatum (blue). The experiments described were performed on hES H9 cell line.

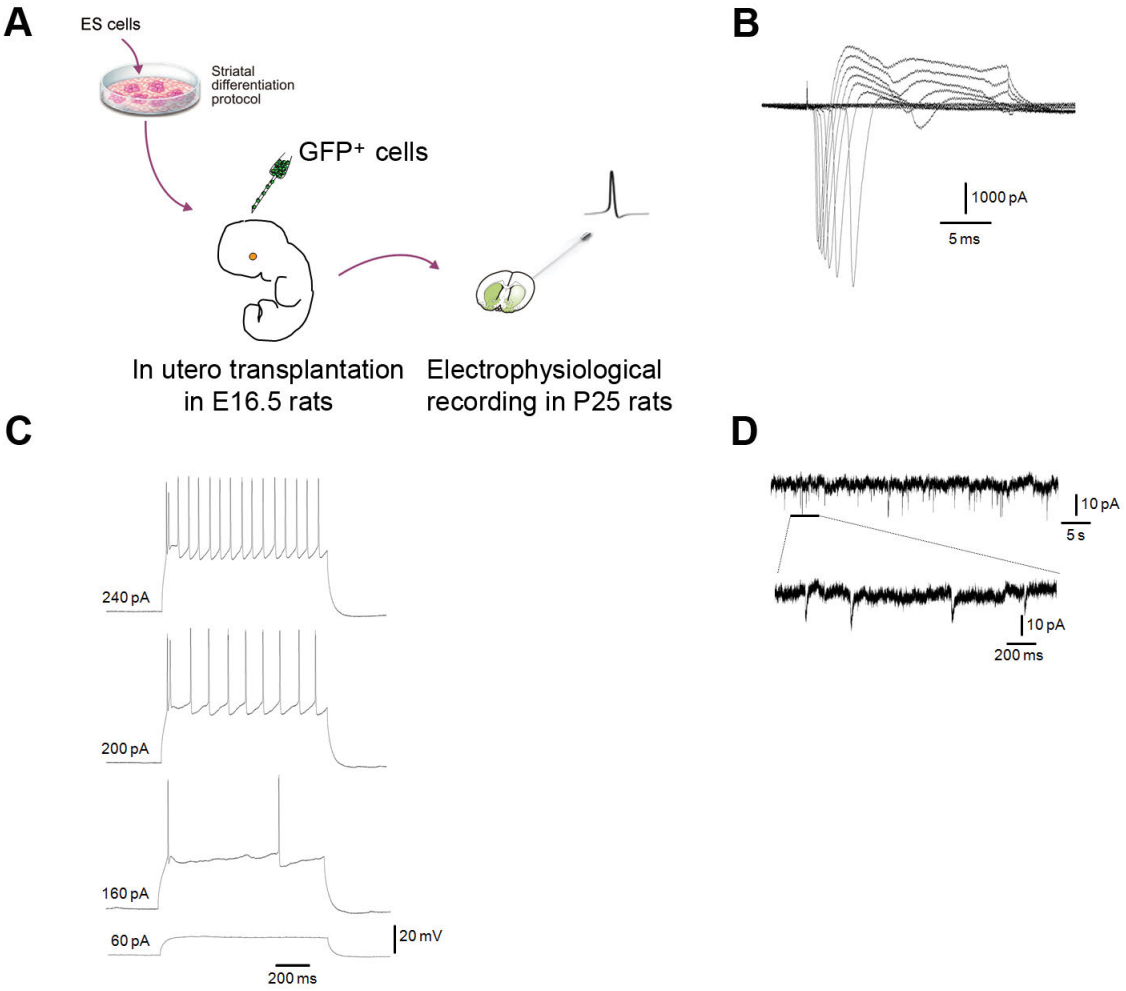

Fig. S12. ***In utero*** **transplanted precursors functionally mature and integrate into the rat brain.** (**A**) Schematic of the transplantation protocol in E16.5 rats. (**B**) I/V relationship. (**C**) Family of sub- and suprathreshold depolarizing steps from the resting potential of –73 mV evoked by injecting rectangular pulses of depolarizing current. Stimulus size is indicated on the left. The cell shows a high frequency of action potentials and a marked after-hyperpolarization. (**D**) Spontaneous postsynaptic currents recorded in voltage-clamp mode at the holding potential of –70 mV.

Table S1. Primer sequences, annealing temperatures and amplicons

Gene	Forward primer	Reverse primer	Ta (°C)	Amplicon (bp)
GAPDH	AGCTGAACGGGAAGCTCACT	AGGTCCACCACTGACACGTTG	60	67
PAX6	TCCATCAGTTCCAACGGAGAA	GTGGAATTGGTTGGTAGACAC	60	337
DACH1	GTGGAAAACACCCCTCAGAA	CTTGTTCCACATTGCACACC	57	208
LIX1	ATGAGTCACTGCCAGCTCCT	GTGGAGGCTACTGCTTCCTG	59	217
LMO3	GGGCTCCACCCTGTACACTA	TAGTCCGTCTGGCAAAGGAT	57	243
MSX1	CCTTCCCTTTAACCCTCACAC	CCGATTTCTCTGCGCTTTTCT	58	285
OTX1	CGTTCACAGCTGGACGTG	CTTTCGGAGCCCGAGCTC	60	230
OTX2	TCAACTTGCCCGAGTCGAGG	CAATGGTCGGGACTGAGGTG	61	204
SIX3	CCGGAAGAGTTGTCCATGTT	CGACTCGTGTTTGTTGATGG	57	171
GBX2	CTCGCTGCTCGCCTTCTC	GCCAGTCAGTCAGATTGTCATCCG	62	173
EMX2	GGGATCCGTCCACCTTCTAC	CTCAAAGGCGTGTTCCAGCC	61	374
FOXP2	GCTTTGACAGTGAGCTAGCTTC	CTGGTGTCACCACTTGATCTTC	58	280
ASCL1	GTCCTGTCGCCCACCATCTC	CCCTCCCAACGCCACTGAC	64	215
FOXG1	TGTTGACTCAGAACTCGCTGG	CTGCTCTGCGAAGTCATTGAC	60	262
DLX5	TTCAGAAGACTCAGTACCTCGC	GAGTTACACGCCATTGGGTC	60	184
DLX6	TACCTCCAGTCCTACCACAAC	AATAAATGGTCCGAGGCTTCCG	60	145
FOXP1	CTACCGCTTCCATGGGAAATC	CTGTTGTCACTAAGGACAGGG	59	207
ISL1	TACAGGCTAACCCAGTGGAAG	GACTGGCTACCATGCTGTTAG	60	207
DrD1	AGGGACATGTCTTTGGCTTCAG	GGGAACAGTGTTAGCACCTGTT	60	173
ARPP21	GTGCAAAGCGTGATGGTTTCC	CCTTGACCTGCCTGGTTAGG	58	128
DARPP-32	CTGAGGACCAAGTGGAAGAC	GATGTCCCCTCCACTTCCTC	58	125
NKX2-1	ACCGGGTTCAGACTCAGTTC	ATCGACATGATTCGGCGTCGG	60	221
EAR	GAGGCTGAGGCAGGAGAATCG	GTCGCCCAGGCTGGAGTG	60	88

Table S2. Antibodies used for immunofluorescence, immunohistochemistry and flow cytometry

Application	Antibody	Dilution	Supplier
Immunofluorescence	OCT4	1:100	Santa Cruz
	OTX2	1:500	Chemicon
	α smooth muscle actin	1:800	Sigma
	GATA4	1:200	Santa Cruz
	p75	1:200	Santa Cruz
	PAX6	1:200	Covance
	nestin	1:200	R&D
	SOX1	1:200	Santa Cruz
	FOXG1	1:1000	StemCulture
	GSX2	1:2000	Gift from Prof. K. Campbell, Cincinnati Children's Hospital Medical Center
	βIII-tubulin	1:1000	Sigma
	MAP2ab	1:500	BD Bioscience
	calbindin	1:200	SWANT
	GABA	1:500	Sigma
	GAD65/67	1:200	Millipore
	FOXP1	1:1000	Abcam
	FOXP2	1:2000	Abcam
	CTIP2	1:500	Abcam
	DARPP-32	1:200	Epitomics
	DRD2	1:200	Millipore
	A2A	1:1000	Upstate
	Synaptophysin	1:200	Sigma
	5-HT	1:500	Sigma
	TH	1:200	Immunological Science
	VGLUT1	1:300	Millipore
	GFAP	1:1000	DAKO
	calretinin	1:200	BD Bioscience
	NPY	1:5000	Immunostar
	parvalbumin	1:500	Chemicon
	somatostatin	1:100	Millipore
	ChAT	1:200	Chemicon
Immunohistochemistry	Human nuclei	1:1000	Millipore
	FOXG1	1:1000	StemCulture
	Human nestin	1:500	Neuromics
	MAP2ab	1:500	Sigma
	Ki67	1:500	DAKO
	N-cadherin	1:100	BD Bioscience
	ZO-1	1:100	Invitrogen
	OTX2	1:1000	Chemicon
	FOXP1	1:500	Abcam
	DARPP-32	1:200	Epitomics
	DARPP-32	1:30,000	Gift from Prof. Hemmings, Cornell University
	α smooth muscle actin	1:500	Sigma
	SOX1	1:150	Santa Cruz
	OCT4	1:100	Santa Cruz
	FOXP2	1:2000	Abcam
	GFAP	1:4000	DAKO
Flow cytometry	OCT4	1:100	Santa Cruz
	OTX2	1:1000	Chemicon
	PAX6	1:5000	Hybridoma Bank
	FOXG1	1:1000	StemCulture

Table S3. Composition of solutions used for electrophysiological recording

Solution	Application	Composition (mM)
1	EXTRACELLULAR: Total currents and voltage signal (neurons in culture)	140 NaCl, 3 KCl, 10 glucose, 10 HEPES, 2 $CaCl_2$, 1 $MgCl_2$ (pH 7.35 with NaOH)
2	INTRACELLULAR: Total currents and voltage signal (neurons in culture)	130 K-gluconate, 4 NaCl, 2 $MgCl_2$, 1 EGTA, 10 HEPES, 5 CP (phosphocreatine), 2 Na_2-ATP, 0.3 Na_3-GTP (pH 7.25 with KOH)
3	INTRACELLULAR: Post-synaptic currents (neurons in culture)	135 CsCl, 3 NaCl, 10 EGTA, 10 HEPES, 0.5 $CaCl_2$, 1 $MgCl_2$, 4 Na_2-ATP, 0.3 Na_3-GTP (pH 7.25 with CsOH)
4	EXTRACELLULAR: Slice preparation (bubbled with 95% O_2/5% CO_2)	70 sucrose, 80 NaCl, 2.5 KCl, 26 $NaHCO_3$, 15 glucose, 1 $CaCl_2$, 7 $MgCl_2$, 1.25 NaH_2PO_4
5	EXTRACELLULAR: aCSF slices (bubbled with 95% O_2/5% CO_2)	125 NaCl, 2.5 KCl, 26 $NaHCO_3$, 15 glucose, 1.3 $MgCl_2$, 2.3 $CaCl_2$, 1.25 $NaHPO_4$